12-2013

Monodentate, Bidentate and Photocrosslinkable Thiol Ligands for Improving Aqueous Biocompatible Quantum Dots

Hiroko Takeuchi
University of Arkansas, Fayetteville

Monodentate, Bidentate and Photocrosslinkable Thiol Ligands for Improving Aqueous Biocompatible Quantum Dots

Monodentate, Bidentate and Photocrosslinkable Thiol Ligands for Improving Aqueous Biocompatible Quantum Dots

A thesis submitted in partial fulfillment
of the requirements for the degree of
Master of Science in Chemistry

By

Hiroko Takeuchi
University of Arkansas
Bachelor of Science in Chemistry, 2010

December 2013
University of Arkansas

This thesis is approved for recommendation to the Graduate Council

_____
Dr. Colin Heyes
Thesis Director

_____
Dr. Jingyi Chen
Committee Member

_____
Dr. Thallapuranam K. Suresh Kumar
Committee Member

ABSTRACT

Water-soluble Quantum Dots (QDs) are highly sensitive fluorescent probes that are often used to study biological species. One of the most common ways to render QDs water-soluble for such applications is to apply hydrophilic thiolated ligands to the QD surface. However, these ligands are labile and can be easily exchanged on the QD surface, which can severely limit their application. As one way to overcome this limitation while maintaining a small colloidal size of QDs, we developed a method to stabilize hydrophilic thiolated ligands on the surface of QDs through the formation of a crosslinked shell using a photocrosslinking approach. This ligand is known to crosslink through ultraviolet (UV) light but, interestingly, our results showed that QD-mediated crosslinking by visible light led to enhanced colloidal stability of the QDs compared to UV light. This was confirmed through spectroscopic, photographic and fluorescence correlation spectroscopy measurements.

In order to maximize the biological applications of QDs, it is important to thoroughly investigate the binding and exchange mechanisms of ligands, and especially how these mechanisms affect the ability to control non-specific adsorption of biomolecules. To investigate this, we modified a near-infrared dye to contain a single thiol group to act as a highly sensitive spectroscopic probe for the binding and exchange of thiol groups to monodentate or bidentate ligand-coated QDs. Differences in how monodentate and bidentate ligands control binding of thiolated target (bio)molecules were discovered by fitting the data to the Hill equation. The results highlight how both the coordination geometry and the ligand packing density on the surface of QDs control the binding and exchange mechanisms. The proposed mechanistic scheme was then successfully tested by exposure to a reduced (i.e. -SH containing) antibody. Finally, Förster Resonance Energy Transfer of QD-dye conjugates was studied. At the single

molecule level three species were identified: QD without a dye bound, QD with 1 dye attached, and QD with 2 or more dyes attached. The unusual statistical distribution of these different species suggests a highly complex process at the microscopic level. These discoveries will contribute to improving the applications of QDs in biophysical and biomedical studies.

ACKNOWLEDGEMENTS

I would like to express my special gratitude to my Master's thesis advisor, Dr. Colin Heyes, who has always been understanding, encouraging, and supportive throughout my graduate years. I am especially grateful for his willingness to share his knowledge and reminding me the significance of my research, which showed me the joy of learning and motivated me to perform better. Without his guidance and advice, I would not be able to have completed a publication, my research projects and this Master's thesis.

I would like to thank Dr. T. K. Suresh Kumar and Dr. Jingyi Chen for serving on my committee. I also would like to thank Dr. Jackson Lay and Dr. Nan Zheng's lab for providing the use of their instruments. Furthermore, I would like to extend my thanks to Dr. Marion Götz from the Department of Chemistry at Whitman College in Washington for synthesizing and providing the diacetylene ligands. I am grateful to have had two postdoctoral researchers in the lab; Dr. Jose Aldana and Dr. Feng Gao, both of who have helped me improve experimental techniques and knowledge of my research field. I also have enjoyed working with the other members of the lab, all of who are very friendly and fun. I hope every single lab member to excel in their careers, and wish them all the best in the future.

My special thanks go to my parents who gave me the opportunity to study abroad in the United States. I feel very fortunate to have studied in such a great environment where I could enhance my knowledge and grow as a person. They have always shown their support and understanding, and encouraged me from home during my graduate years. Lastly, I would like to express my regards to all of those people who supported me in any respect during the completion of the project.

TABLE OF CONTENTS

I. Chapter 1: Introduction
- 1.1 Quantum Dots (QDs) 1
- 1.2 Advantages of QDs over Organic Dyes 2
- 1.3 Characterization of QDs 3
- 1.4 Surface coating of QDs for Biocompatibility 6
- 1.5 Objectives and Approaches 8
- 1.6 References 10

II. Chapter 2: Crosslinking of Bifunctional Diacetylene Ligands on Aqueous QDs 14
- 2.1 Introduction 14
- 2.2 Experimental Methods 14
  - 2.2.1 *Ligand Exchange with Photocrosslinkable Diacetylene* 14
  - 2.2.2 *Optimizing UV Exposure Time* 15
  - 2.2.3 *Photocrosslinking* 16
  - 2.2.4 *Colloidal Stability Test* 17
  - 2.2.5 *Fluorescence Correlation Spectroscopy (FCS)* 17
- 2.3 Results and Discussion 18
  - 2.3.1 *Water Soluble QDs* 18
  - 2.3.2 *Photocrosslinking Results* 19
  - 2.3.3 *Stability of Diacetylene Capped QDs* 22
  - 2.3.4 *Fluorescence Correlation Spectrophotometry (FCS)* 25
- 2.4 Conclusion 29
- 2.5 References 30

III. Chapter 3: Are Bidentate Ligands Really Better than Monodentate Ligands For Nanoparticles? 33
- 3.1 References 58
- 3.2 Appendix I 61
- 3.3 Appendix II 62

IV. Chapter 4: Ensemble and Single Molecule Spectroscopic Analyses of QD-Dye Conjugates 63
- 4.1 Introduction 63
- 4.2 Experimental Methods 63
  - 4.2.1 *Photoluminescence (PL)* 63
  - 4.2.2 *Fluorescence Lifetime* 64
- 4.3 Results and Discussion 65
  - 4.3.1 *Photoluminescence (PL)* 65
  - 4.3.1 *Single Molecule Spectroscopy* 67
- 4.4 Conclusion 70
- 4.5 References 71

V. Chapter 5: Conclusions 73

LIST OF PUBLICATIONS

Hiroko Takeuchi, Benard Omogo, and Colin D. Heyes. Are Bidentate Ligands Really Better than Monodentate Ligands For Nanoparticles? Nano Letters, 2013, 13 (10), pp 4746-4752.

LIST OF ABBREVIATIONS

ACF	Autocorrelation Function
CdSe	Cadmium Selenide
CdTe	Cadmium Telluride
DA	Diacetylene
DHLA	Dihydrolipoic Acid
EDTA	Ethylenediaminetetraacetic Acid
FCS	Fluorescence Correlation Spectroscopy
FRET	Förster Resonance Energy Transfer
FT-IR	Fourier Transform Infrared
FWHM	Full Width at Half Maximum
HPLC	High Performance Liquid Chromatography
IgG	Immunoglobulin G
MALDI-TOF	Matrix Assisted Laser Desorption-Ionization Time-Of-Flight
ML	Monolayer
MPA	Mercaptopropionic Acid
NMR	Nuclear Magnetic Resonance
ODA	Octadecylamine
PBS	Phosphate Buffered Saline
PDA	Polydiacetylene
PL	Photoluminescence
PSF	Point Spread Function
PVA	Poly Vinyl Alcohol

QD	Quantum Dot
SATA	N-Succinimidyl S-Acetylthioacetate
TCEP	Tris(2-carboxyethyl)phosphine
TCSPC	Time-Correlated Single Photon Counting
TEM	Transmission Electron Microscopy
TMAOH	Tetramethylammonium Hydroxide Pentahydrate
UV	Ultraviolet
UV-Vis	Ultraviolet-Visible
ZnS	Zinc Sulfide

Chapter 1: Introduction

1.1 Quantum Dots (QDs)

Colloidal semiconductor nanocrystals, also known as quantum dots (QDs) are single crystals whose size and shape can be controlled by types of materials and the synthesis conditions.[1] When the size of QDs become smaller than the Bohr exciton radius (a few nanometers), quantum confinement effects are observed. Quantum confinement is explained as a phenomenon whereby as the QD sizes decreases, as their band gap - the energy difference between the conduction bands and valance bands - increases in energy (**Figure 1.1**). Therefore, the QDs undergo a 'blue shift' in the absorption and emission spectra as their sizes become smaller. QDs are characterized by unique optical properties such as board absorption, narrow and symmetric emission bands, size-tunable photoluminescence, high quantum yield (as high as 90 %), and long fluorescence lifetime. [1-4] These properties have attracted researchers to employ them as better fluorescent probes over conventional organic fluorophores for long term and highly sensitive fluorescence imaging.

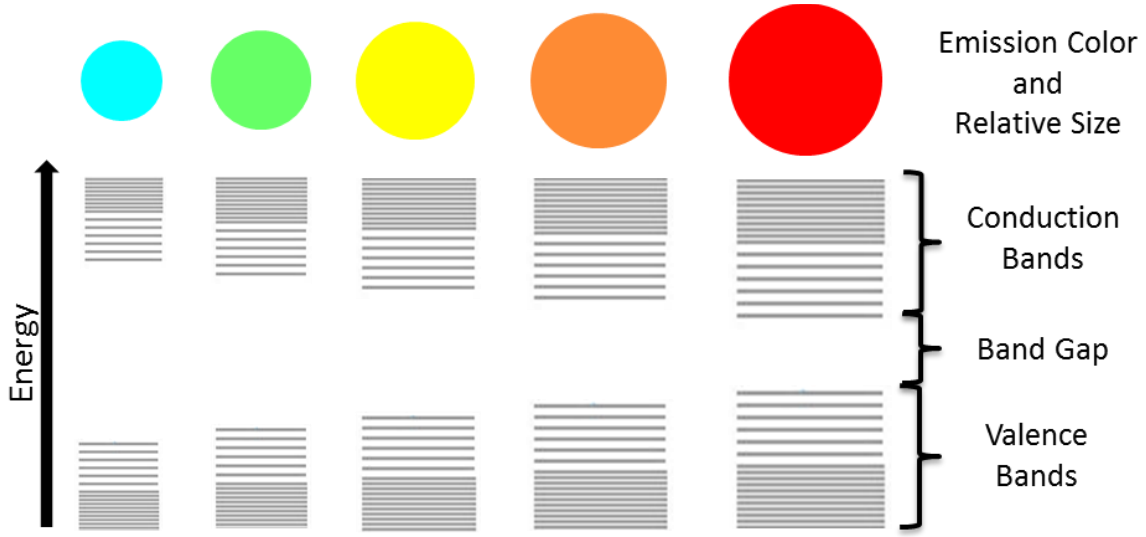

Figure 1.1: Relationship between size of QDs and their band gap between the conduction band and valence band as explained by quantum confinement.

The type of QDs commonly used as fluorescent labels are easily synthesized, as well as being commercially available, and are based on CdSe/ZnS core/shell semiconductor nanocrystals. CdSe cores are particularly useful as, between the relatively small sizes of 2-6 nm, cover the visible light region. Coating the CdSe core with higher band gap materials, such as ZnS shells, has a couple of significant advantages. By shell passivation, the optically-active core is protected from the surrounding environment, which leads to its improved stability against photodegradation. Also, the charge carriers are better confined in the core by the larger band gap of ZnS, both reducing non-radiative relaxation pathways at the surface and increasing the overlap of the delocalized excited electron and hole wavefunctions, thereby improving the fluorescence quantum yield. Upon shelling the core, a small red shift of excitonic peak is typically observed in absorption and photoluminescence (PL) spectra, due to tunneling of the electron wavefunction into the shell.[5] Moreover, when CdSe core is water-solubilized with thiol ligands, its fluorescence is quenched more than CdSe/ZnS core/shell in water.[6]

1.2 Advantages of QDs over Organic Dyes

The development of fluorophores in general has been beneficial in labeling proteins in living cells and studying the functions and interactions of various biomolecules. However, there are some obstacles with using organic fluorophores, particularly regarding their ability to easily photobleach. Photo-instability of organic dyes has been compared to the more photo-stable QDs and it has been uncovered that the fluorescence of green molecular fluorophores quenched to about 5% within one minute of 100 W mercury lamp exposure whereas QDs showed unquenched brightness for the full 3 minutes examined.[7] Another attractive feature of QDs is the gradual increase in the absorption toward shorter wavelength, independent to their size, resulting

in a broad excitation profile. This enables the excitation of various sizes (colors) of QDs to provide multi-color fluorescence studies by using a single illumination source.[8] This broad absorption also provides more choices of excitation wavelength, compared to narrower choices of excitation wavelength for dyes, leading to compatibility with a wide range of experimental setups.[9] Another advantage of QDs is to be able to tune their emission to the near-infrared region to avoid cellular auto fluorescence during cellular imaging simply by increasing their size.[10] There are organic fluorophores that fluoresce at near-infrared; however, their quantum yield is rather limited at this region, and their photostability is even worse than visible light organic fluorophores. Due to these promising benefits of using QDs as fluorescing probes, pioneering work in 1998 brought them to the attention of many biophysicists and molecular biologists.[11, 12]

1.3 Characterization of QDs

One of the most important initial QD characterization methods is Ultraviolet-visible (UV-Vis) absorption spectrophotometry, which measures the energy absorbed by an electron as it is excited to the conduction band from the valence band. The absorption spectrum also allows one to calculate the concentration of QDs (c) in molarity since absorption (A), as defined by the Beer's law:

$$A = cl\varepsilon \qquad (\mathbf{1.1})$$

where l is a path length in centimeter, and ε is extinction coefficient in $cm^{-1}M^{-1}$. The extinction coefficient at a certain wavelength indicates the probability that a species will absorb a photon of that wavelength. The extinction coefficient of the first excitonic peak at the band edge is known to increase in value as the size of CdSe core increases.[13]

Photoluminescence (PL) spectrometry is another common characterization method for QDs. As the exciton relaxes back to the ground state, the absorbed energy is released either radiatively or non-radiatively. PL spectra are useful in determining both quantum yields of QDs, from their PL intensity, and, since an emitted photon depends on the size of the QD, the size dispersity of the sample can be estimated from the width of the PL peak (commonly measured as the full width at half maximum, FWHM).

The narrow and tunable emission spectra of QDs are advantageous in Förster Resonance Energy Transfer (FRET) studies, where the non-radiative transfer of excitation energy from a fluorescent donor to a proximal acceptor. FRET efficiency (E) has a strong dependence on donor-acceptor separation distance, d ($E \sim 1/d^6$) and on the spectral overlap between the acceptor absorption and the donor emission, and can be measured as the decrease in fluorescence intensity in the presence of the acceptor. Due to the distance dependency, this measurement has become a popular diagnostic tool for conformational changes in biomolecules as well as measuring molecular interactions, with its sensitivity ranging between 20 and 100 Å. As discussed above, the QDs' absorption spectra show broad bands, which enables one to separate the excitation of the QD donor from the absorption of the dye acceptor, which are typically applied in biophysical studies. [14-16] Using organic dye donor-acceptor pairs for FRET studies is often used, but the narrower absorption spectra and wider emission spectra leads to both cross-talk, caused by spectral overlap of the donor into the acceptor emission region, and difficult-to-avoid direct excitation of the acceptor dye, leading to technical limitations.[17] Therefore, the option of using various well-separated excitation wavelengths and the tunable, narrow emission of QDs makes them great candidates for use as FRET donors.

FRET efficiency can also be measured by the fluorescence lifetime of the QD donor. The fluorescence lifetime is the average delay time between fluorescence emission and excitation. For QDs, lifetimes are usually greater than 10 ns, whereas molecular fluorophores are usually less than 5 ns, which leads to QDs being particularly beneficial for imaging biological samples, since autofluorescence in cells is usually also around 3-5 ns, and enables one to separate QD signals from autofluorescence signals. In the presence of an acceptor, the fluorescence lifetime decreases due to the FRET process competing with the emission process, and depends on the number of acceptors; if there are more acceptors in close proximity to a donor, its fluorescence lifetime becomes shorter.[18]

In addition to these ensemble fluorescence spectroscopy analyses, they can be characterized at the single particle level. At the ensemble level, the average value for a large numbers of QDs is reported; however, at single molecular level, the distributions of individual values can be obtained, thereby relaying much more information than the ensemble-averaged signal. Additionally, unsynchronized events such as blinking – the flickering of the fluorescence signal between on and off states – can be observed from single QDs. [18-20] The mechanism of blinking is still under investigation, but its effect can severely limit the applications of QDs. Another important characterization at the single molecular level is to monitor aggregation and diffusion of QDs, which is especially important in determining the colloidal stability of QDs. By using fluorescence correlation spectroscopy (FCS), the signal fluctuation of particles diffusing in and out of a focused beam can be measured. Through mathematical interpretation, the diffusion time (τ_D) and the hydrodynamic radius (r) can be extracted. A slow diffusion time, and thus increase in hydrodynamic radius, indicates the formation of QD aggregates.

1.4 Surface coating of QDs for Biocompatibility

In order to apply QDs as fluorescent probes in biological research, they need to be water-soluble. However, the synthesis of bright fluorescing QDs usually takes place in organic solvents in the presence of hydrophobic surfactants; QDs synthesis in aqueous solutions usually results in lower quantum yields compared to those synthesized in organic solvent. Therefore, the hydrophobic surface coating of QDs needs to be modified to gain water-solubility. Various strategies have been invented to engineer water-soluble QDs, which has been summarized in several review articles.[1, 9, 21-23] The methods can be categorized into two major types: one is to remove the original hydrophobic ligands on the surface of QDs and replace them with hydrophilic ligands, called ligand exchange. The other type is to apply another coating, usually an amphiphilic polymer, over the original organic ligands, relying on hydrophobic interactions between the ligands[7, 24, 25]. This latter method tends to result in the increase in the colloidal size of water-soluble QDs, compared to the shorter hydrophilic ligands that can be used in ligand exchange. The most frequently used hydrophilic ligands contain thiol (-SH) group at one end of the molecule for binding to the surface of QDs and a carboxylic (-COOH) functional group on the other end to impart water-solubility and potential reactivity for conjugating to biomolecules. Examples of such mercaptocarboxylic acids are: monothiol ligands[11, 26-28] (e.g. marcaptopropionic acid, MPA), dithiol dihydrolipoic acid (DHLA)[29-31], and crosslinkable mercaptopropyl silanol[12, 32]. Di- or multi-thiolated ligands have been shown to increase the colloidal stability compared to mono-thiolated ligands.[29, 30, 33] In the latter, silica shell capping produces higher colloidal stabilities but results in larger hydrophilic QDs sizes whereas MPA and DHLA coated QDs remain small in size.

In order to facilitate the idea of crosslinking, water-solubilizing ligands to engineer more stable QDs in water, but still resulting in small hydrophilic QDs size, diacetylene (DA) containing thiol ligand could be an alternative candidate. Diacetylene is known to photocrosslink upon UV-exposure (at 254 nm) and has been used to form self-assembling monolayers on gold surfaces. [34, 35] In fact, the diacetylene capping to a gold spherical nanoparticle has been recently explored.[36] Even though the colloidal stability analysis on DA capped gold nanoparticles was not examined, the application of DA as water-solubilizing ligand on QDs for bioimaging seems promising, and will be investigated in chapter 2.

In order to use these stable and small-sized water-soluble QDs, it is important to gain control of the conjugation of QDs to targeting molecules for fluorescing imaging, which is achieved by gaining control in the number of binding sites on the surface of QDs through the ligand exchange reaction. It is possible to gain a better control of the site-specific conjugation of QDs with biomolecules by introducing a thiol-reactive bifunctional linker which specifically forms a covalent bond to a thiol group of the typically low abundant cysteine amino acid. However, there is a potential direct nonspecific binding of the cysteine thiol group to the surface of QDs. Therefore, it is essential to understand and quantize the nonspecific and specific ligand binding and exchange process. Such a ligand exchange process has not yet been quantified, especially for core/shell CdSe/ZnS QDs. There have been some studies exploring the characterization of CdSe-surface ligand interactions by measuring the fluorescence intensity and lifetime during the ligand exchange, since it is known that thiol groups on the surface of the core can act as an electron hole trap and reduces QDs emission.[37, 38] NMR spectroscopy has also been used to monitor the relative intensity of ligands on the surface of QDs, but this is a low sensitivity technique and the requirement of high concentrations of material are still a major

drawback.[39] The use of radioactive labeling of ligands with tritium has been also employed to quantify the number of ligands on the surface of CdSe QDs; however, the application of this method to aqueous solution is not yet reported.[40] Therefore, quantifying commonly-used water-solubilizing ligand interactions with the surface of QDs at high sensitivity is still a pressing need, especially in relating how thiolated target molecules compete with such ligands on the QD surface.

1.5 Objectives and Approaches

In this thesis, bright, photostable, water-soluble CdSe/ZnS quantum dots are synthesized by coating with diacetylene-containing ligands for possible applications in biophysical studies (Chapter 2). Moreover, in order to gain control of the bioconjugation process, ligand binding and exchange on the surface of QDs has been explored as a function of ligand coordination geometry (Chapter 3 and 4).

The synthesis of DA-capped QDs is illustrated in **Figure 1.2**. In order to maximize the photocrosslinking process for DA ligands after ligand exchange, red emitting (larger) QDs are used, which reduces the curvature of the surface caused by the spherical shape and thus enabling closer packing of DA ligands. As-purchased QDs contained octadecylamine (ODA) ligands as the original hydrophobic ligands. A ligand exchange reaction was performed using DA and MPA to compare the colloidal stability of the resulting water-solubilized QDs. The colloidal stability was measured under continuous room light exposure with periodical absorption measurements and observations by photographs. Quantitative analysis was performed using fluorescence correlation spectroscopy.

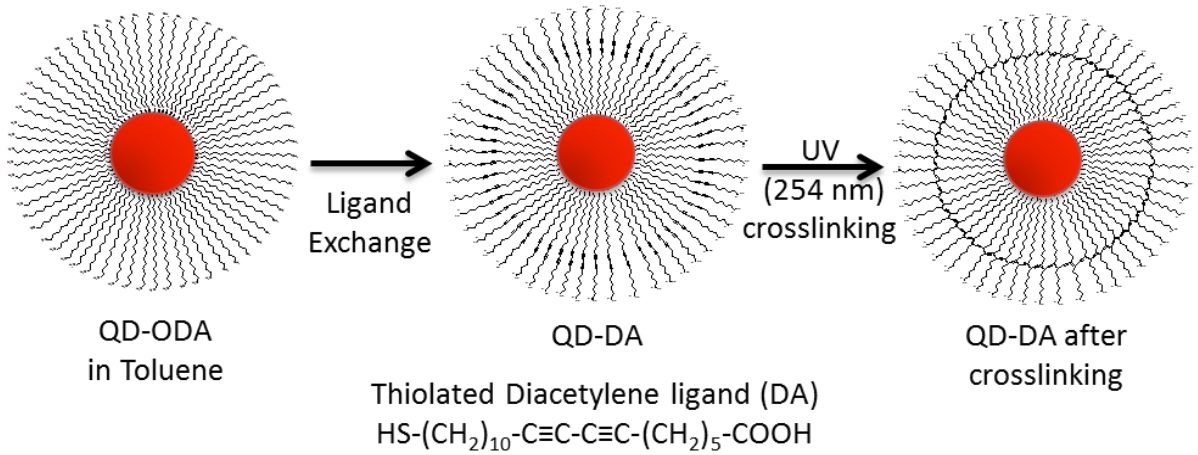

Figure 1.2: Reaction scheme for synthesis of crosslinked DA capped QDs, together with the structural formula of our DA ligand.

The study of ligand binding and exchange as a function of thiol coordination geometry employed commercially-available green-emitting (smaller) QDs. The reaction scheme is shown in **Figure 3.4**. The two different types of binding coordination between water-solubilizing ligands and the surface of QDs were employed. It is generally agreed that multidentate coordination leads to better colloidal stability than monodentate ligands.[29, 41] However, there is much less knowledge on how these ligands affect the binding of thiolated target molecules to QD surfaces thus leading us to pose the question, "Are Bidentate Ligands Really Better than Monodentate Ligands For Nanoparticles?" To answer this question, the commonly used ligands, MPA (monodentate) and DHLA (bidentate), were introduced during ligand exchange to uncover the differences in binding and exchange for monodentate and bidentate thiol linkages to the surface of QDs. In order to monitor the exchange reaction, we engineered a novel fluorescing reporter by modifying a fluorophore to have a single thiol group as an exchanging ligand. Having completed the exchange by mixing the thiolated dye with water-soluble QDs at various molar ratios, the conjugates were purified using size exclusion columns and analyzed by absorption, PL, FRET, and fluorescence lifetime spectroscopy.

1.6 References

1. Michalet, X.; Pinaud, F. F.; Bentolila, L. A.; Tsay, J. M.; Doose, S.; Li, J. J.; Sundaresan, G.; Wu, A. M.; Gambhir, S. S.; Weiss, S., Quantum Dots for Live Cells, in Vivo Imaging, and Diagnostics. *Science (Washington, DC, U. S.)* 2005, 307, 538-544.

2. Pinaud, F.; Michalet, X.; Bentolila, L. A.; Tsay, J. M.; Doose, S.; Li, J. J.; Iyer, G.; Weiss, S., Advances in fluorescence imaging with quantum dot bio-probes. *Biomaterials* 2006, 27, 1679-1687.

3. Reiss, P.; Protiere, M.; Li, L., Core/Shell Semiconductor Nanocrystals. *Small* 2009, 5, 154-168.

4. Torchynska, T.; Vorobiev, Y., Semiconductor II-VI Quantum Dots with Interface States and Their Biomedical Applications. 2011.

5. Dabbousi, B. O.; RodriguezViejo, J.; Mikulec, F. V.; Heine, J. R.; Mattoussi, H.; Ober, R.; Jensen, K. F.; Bawendi, M. G., (CdSe)ZnS core-shell quantum dots: Synthesis and characterization of a size series of highly luminescent nanocrystallites. *Journal of Physical Chemistry B* 1997, 101, 9463-9475.

6. Kloepfer, J. A.; Bradforth, S. E.; Nadeau, J. L., Photophysical Properties of Biologically Compatible CdSe Quantum Dot Structures. *The Journal of Physical Chemistry B* 2005, 109, 9996-10003.

7. Wu, X. Y.; Liu, H. J.; Liu, J. Q.; Haley, K. N.; Treadway, J. A.; Larson, J. P.; Ge, N. F.; Peale, F.; Bruchez, M. P., Immunofluorescent labeling of cancer marker Her2 and other cellular targets with semiconductor quantum dots. *Nature Biotechnology* 2003, 21, 41-46.

8. Yi-Ping, H.; Kung, M. C.; Yang, S.; Tza-Huei, W., Multiplexed hybridization detection with multicolor colocalization of quantum dot nanoprobes. *Nano Letters* 2005, 5, 1693-1697.

9. Resch-Genger, U.; Grabolle, M.; Cavaliere-Jaricot, S.; Nitschke, R.; Nann, T., Quantum dots versus organic dyes as fluorescent labels. *Nature Methods* 2008, 5, 763-775.

10. Kim, S.; Lim, Y. T.; Soltesz, E. G.; De Grand, A. M.; Lee, J.; Nakayama, A.; Parker, J. A.; Mihaljevic, T.; Laurence, R. G.; Dor, D. M.; Cohn, L. H.; Bawendi, M. G.; Frangioni, J. V., Near-infrared fluorescent type II quantum dots for sentinel lymph node mapping. *Nature Biotechnology* 2004, 22, 93-97.

11. Chan, W. C. W.; Nile, S., Quantum dot bioconjugates for ultrasensitive nonisotopic detection. *Science (Washington, D. C.)* 1998, 281, 2016-2018.

12. Bruchez, M., Jr.; Moronne, M.; Gin, P.; Weiss, S.; Alivisatos, A. P., Semiconductor nanocrystals as fluorescent biological labels. *Science (Washington, D. C.)* 1998, 281, 2013-2016.

13. Yu, W. W.; Qu, L. H.; Guo, W. Z.; Peng, X. G., Experimental determination of the extinction coefficient of CdTe, CdSe, and CdS nanocrystals. *Chemistry of Materials* 2003, 15, 2854-2860.

14. Clapp, A. R.; Medintz, I. L.; Mauro, J. M.; Fisher, B. R.; Bawendi, M. G.; Mattoussi, H., Fluorescence resonance energy transfer between quantum dot donors and dye-labeled protein acceptors. *Journal of the American Chemical Society* 2004, 126, 301-310.

15. Clapp, A. R.; Medintz, I. L.; Uyeda, H. T.; Fisher, B. R.; Goldman, E. R.; Bawendi, M. G.; Mattoussi, H., Quantum dot-based multiplexed fluorescence resonance energy transfer. *Journal of the American Chemical Society* 2005, 127, 18212-18221.

16. Shivkumar, M. A.; Inamdar (Doddamani), L. S.; Rabinal, M. H. K.; Mulimani, B. G.; Advi Rao, G. M.; Inamdar, S. R., FRET from CdSe/ZnS Core-Shell Quantum Dots to Fluorescein 27 Dye. *Open Journal of Physical Chemistry* 2013, 3, 9.

17. Willard, D. M.; Carillo, L. L.; Jung, J.; Van Orden, A., CdSe-ZnS quantum dots as resonance energy transfer donors in a model protein-protein binding assay. *Nano Letters* 2001, 1, 469-474.

18. Fomenko, V.; Nesbitt, D. J., Solution Control of Radiative and Nonradiative Lifetimes: A Novel Contribution to Quantum Dot Blinking Suppression. *Nano Letters* 2007, 8, 287-293.

19. Durisic, N.; Godin, A. G.; Walters, D.; Grutter, P.; Wiseman, P. W.; Heyes, C. D., Probing the "Dark" Fraction of Core-Shell Quantum Dots by Ensemble and Single Particle pH-Dependent Spectroscopy. *Acs Nano* 2011, 5, 9062-9073.

20. Ebenstein, Y.; Mokari, T.; Banin, U., Fluorescence quantum yield of CdSe/ZnS nanocrystals investigated by correlated atomic-force and single-particle fluorescence microscopy. *Applied Physics Letters* 2002, 80, 4033-4035.

21. Medintz, I. L.; Uyeda, H. T.; Goldman, E. R.; Mattoussi, H., Quantum dot bioconjugates for imaging, labelling and sensing. *Nature Materials* 2005, 4, 435-446.

22. Mazumder, S.; Dey, R.; Mitra, M. K.; Mukherjee, S.; Das, G. C., Review: Biofunctionalized Quantum Dots in Biology and Medicine. *Journal of Nanomaterials* 2009, 17.

23. Yu, W. W.; Chang, E.; Drezek, R.; Colvin, V. L., Water-soluble quantum dots for biomedical applications. *Biochem. Biophys. Res. Commun.* 2006, 348, 781-786.

24. Anderson, R. E.; Chan, W. C. W., Systematic Investigation of Preparing Biocompatible, Single, and Small ZnS-Capped CdSe Quantum Dots with Amphiphilic Polymers. *ACS Nano* 2008, 2, 1341-1352.

25. Gao, X.; Cui, Y.; Levenson, R. M.; Chung, L. W. K.; Nie, S., In vivo cancer targeting and imaging with semiconductor quantum dots. *Nat. Biotechnol.* 2004, 22, 969-976.

26. Zeng, T.; Hu, Y. X.; Wang, N.; Xia, C. Q.; Li, S. J.; Zu, Y.; Liu, L.; Yao, Z. Y.; Zhao, Y. L.; Wu, H. C., Effects of different metal ions on the fluorescence of CdSe/ZnS quantum dots capped with various thiolate ligands. *Physical Chemistry Chemical Physics* 2013, 15, 18710-18715.

27. Aguilera-Sigalat, J.; Rocton, S.; Sanchez-Royo, J. F.; Galian, R. E.; Perez-Prieto, J., Highly fluorescent and photostable organic- and water-soluble CdSe/ZnS core-shell quantum dots capped with thiols. *Rsc Advances* 2012, 2, 1632-1638.

28. Xuefeng, L.; Yan, G.; Xiaomin, W.; Shaojue, W.; Zhiyong, T., Preparation of stable, water-soluble, highly luminescence quantum dots with small hydrodynamic sizes. *Journal of Nanoscience and Nanotechnology* 2011, 11, 1941-1949.

29. Uyeda, H. T.; Medintz, I. L.; Jaiswal, J. K.; Simon, S. M.; Mattoussi, H., Synthesis of compact multidentate ligands to prepare stable hydrophilic quantum dot fluorophores. *Journal of the American Chemical Society* 2005, 127, 3870-3878.

30. Mattoussi, H.; Mauro, J. M.; Goldman, E. R.; Anderson, G. P.; Sundar, V. C.; Mikulec, F. V.; Bawendi, M. G., Self-assembly of CdSe-ZnS quantum dot bioconjugates using an engineered recombinant protein. *Journal of the American Chemical Society* 2000, 122, 12142-12150.

31. Clapp, A. R.; Goldman, E. R.; Mattoussi, H., Capping of CdSe-ZnS quantum dots with DHLA and subsequent conjugation with proteins. *Nat. Protoc.* 2006, 1, 1258-1267.

32. Gerion, D.; Pinaud, F.; Williams, S. C.; Parak, W. J.; Zanchet, D.; Weiss, S.; Alivisatos, A. P., Synthesis and properties of biocompatible water-soluble silica-coated CdSe/ZnS semiconductor quantum dots. *Journal of Physical Chemistry B* 2001, 105, 8861-8871.

33. Pinaud, F.; King, D.; Moore, H.-P.; Weiss, S., Bioactivation and Cell Targeting of Semiconductor CdSe/ZnS Nanocrystals with Phytochelatin-Related Peptides. *J. Am. Chem. Soc.* 2004, 126, 6115-6123.

34. Kim, T. S.; Crooks, R. M.; Tsen, M.; Sun, L., Polymeric Self-Assembled Mnolayers. 2. Synthesis and Characterization of Self-Assembled Polydiacetylene Monolayers and Multilayers. *Journal of the American Chemical Society* 1995, 117, 3963-3967.

35. Kim, T.; Ye, Q.; Sun, L.; Chan, K. C.; Crooks, R. M., Polymeric self-assembled monolayers .5. Synthesis and characterization of omega-functionalized, self-assembled diacetylenic and polydiacetylenic monolayers. *Langmuir* 1996, 12, 6065-6073.

36. Alloisio, M.; Demartini, A.; Cuniberti, C.; Muniz-Miranda, M.; Giorgetti, E.; Giusti, A.; Dellepiane, G., Photopolymerization of diacetylene-capped gold nanoparticles. *Physical Chemistry Chemical Physics* 2008, 10, 2214-2220.

37. Breus, V. V.; Heyes, C. D.; Nienhaus, G. U., Quenching of CdSe-ZnS Core-Shell Quantum Dot Luminescence by Water-Soluble Thiolated Ligands. *Journal of Physical Chemistry C* 2007, 111, 18589-18594.

38. Koole, R.; Schapotschnikow, P.; Donega, C. D.; Vlugt, T. J. H.; Meijerink, A., Time-dependent photoluminescence spectroscopy as a tool to measure the ligand exchange kinetics on a quantum dot surface. *Acs Nano* 2008, 2, 1703-1714.

39. Aldana, J.; Wang, Y. A.; Peng, X., Photochemical Instability of CdSe Nanocrystals Coated by Hydrophilic Thiols. *J. Am. Chem. Soc.* 2001, 123, 8844-8850.

40. Knittel, F.; Gravel, E.; Cassette, E.; Pons, T.; Pillon, F.; Dubertret, B.; Doris, E., On the Characterization of the Surface Chemistry of Quantum Dots. *Nano Letters* 2013, 13, 5075-5078.

41. Susumu, K.; Mei, B. C.; Mattoussi, H., Multifunctional ligands based on dihydrolipoic acid and polyethylene glycol to promote biocompatibility of quantum dots. *Nature Protocols* 2009, 4, 424-436.

Chapter 2: Crosslinking of Bifunctional Diacetylene Ligands on Aqueous QDs

2.1 Introduction

In this part of the research our aim was to enhance the colloidal stability of QDs by coating with crosslinked surfactants, which was achieved by crosslinking thiolated ligands that had been ligand-exchanged onto QDs. It has been shown that diacetylene groups can be photopolymerized upon 254 nm UV exposure.[1-5] This project was performed in collaboration with the Dr. Götz lab, from the Department of Chemistry at Whitman College, who synthesized photocrosslinkable thiolated diacetylene (DA) ligands. The ligands were stored in the freezer until the ligand exchange reaction was performed. Absorbance and fluorescence spectra were measured after each of the following steps; before and after ligand exchange and photopolymerization with either UV or visible light. As a control, QDs were also water-solubilized with the mercaptopropionic acid (QD-MPA) under the same conditions. Having recorded the colloidal stability over a period of 2 weeks by photography, quantitative characterization of QD-DA aggregation was operated through single molecule spectroscopy.

2.2 Experimental Methods

2.2.1 *Ligand Exchange with Photocrosslinkable Diacetylene*

The CdSe/ZnS core/shell quantum dots (QDs) were purchased from Ocean NanoTech in dried powder form. The QDs (λ_{em}=597 nm) were coated with organic octadecylamine (ODA) ligands. Prior to the ligand exchange, as purchased QDs were dissolved in toluene and purified by precipitating from toluene with acetone, centrifuging at 14,100 g (14.5000 rpm on a Centrifuge MiniSpin plus, Eppendorf) for 30 minutes and discarding the non-fluorescing

supernatant. The excess original ODA ligands were removed by re-dissolving the precipitated QDs into hexane and mixing with methanol, followed by 30 minutes of centrifugation at 14,100 g. Having discarded the supernatant, the QDs were purged with Argon to prevent oxidation.

The ligand solution was prepared by adding 1 mL of DriSolv® chloroform (EMD) into a glass vial containing approximately 10 mg of the thiolated diacetylene ligand. The pH was adjusted to 11 by adding 200 μL of 0.625 M tetramethylammonium hydroxide pentahydrate (TMAOH) in methanol. The clear yellow ligand solution was added to the dried QDs and was stirred for 24 hours at room temperature in the dark. A molar ratio of 1 to 100,000 of QDs to diacetylene ligands was applied in this reaction.

As a control, QD-MPA was synthesized using a similar technique as described above. QDs were purified, and ODAs were removed using the same method. The MPA ligand solution was prepared by obtaining 2.66 μL of MPA in 1 mL of methanol and 30 μL of 2.5 M TMAOH methanol solution, resulting in pH=11. The MPA ligand solution was poured into the purified QDs, and the mixture was stirred for a day at ambient temperature under light exclusion. The molar ratio between QD and MPA was 1:20,000.

Optical properties of QDs were checked before and after the ligand exchange with either DA or MPA by UV-Vis spectrometry and fluorometer in an Ultra-Micro cuvette.

2.2.2 *Optimizing UV Exposure Time*

The optimal UV exposure time was determined by monitoring fluorescence of the sample as the function of the UV exposure time over 3.5 hours. From the QD-DA solution in chloroform, 200 μL of the solution that was under continuous UV exposure was taken out of the reaction vial periodically until the solution ran out.

Emission spectra of each sample were obtained by exciting at 530 nm in an Ultra-Micro fluorometer cell. Changes in the emission peak intensity from the same sample were observed when left in the instrument for a period of time, which we attributed to be due to the excitation beam from the fluorometer. Therefore, PL spectra of each sample were taken several times to monitor the emission intensity trend under visible light.

Samples illuminated for 0 minute, 20 minutes, 100 minutes and 210 minutes were analyzed using Fourier transform infrared (FT-IR) spectroscopy (Bruker, Vertex 70) to monitor the formation of polydiacetylene (PDA). The crosslinking of DA could be confirmed by monitoring the transmission peak of the triple bonds (2200~2400cm^{-1}) whose intensity should decrease as PDA was formed. The FT-IR samples were prepared by drying each sample on a CaF_2 window (Harrick Scientific, WFD-U22) under N_2. The baseline was taken with chloroform, and each sample was scanned 16 times and averaged to obtain the spectra.

2.2.3 ***Photocrosslinking***

In order to compare the effect of UV exposure on crosslinking, both QD-DA and QD-MPA samples were divided into two different 1.8mL glass vials: one for UV exposure and the other for non-UV exposure as a control. The sample vials were directly placed on a hand-held UV-light (254 nm) for 30 minutes without any interference of ambient light. The non-UV exposed sample vials were wrapped with aluminum foil and placed on the UV-light during this process.

In order to monitor the stability in the environment that was close to biological conditions, all water-soluble QD-DA and QD-MPA were transferred to water by adding methanol and acetone, respectively, and centrifuging at 14,100 g on MiniSpin to precipitate out from the reaction solution. Having removed a supernatant, QDs were re-dissolved into 200 μL of

Millipore (18.2 MΩ.cm) water. Each solution was transferred to a 4-windowed semi-micro fluorometer cells with a stopper (Sterna Cells, 29F-Q-10) for further analysis.

2.2.4 *Colloidal Stability Test*

The colloidal stability of the final products was tested by leaving the samples under ambient light continuously in 4-windowed semi-micro fluorometer cells with a stopper. Observation of fluorescence under a handheld UV light at 366 nm and absorption was monitored periodically by taking images with a 10.5 MP camera (Pentax) and a UV-Vis spectrophotometer, respectively. For each measurement, the product solution was carefully handled to avoid shaking the solution so that the aggregates were not included in the absorption spectra. The test was continued for two weeks until the stability difference became apparent between the four samples.

2.2.5 *Fluorescence Correlation Spectroscopy (FCS)*

Having completed the stability test, QD-DA samples were further analyzed by measuring the fluorescence in a single molecule burst experiment followed by lifetime and FCS analysis. The data was acquired on a Picoquant Microtime 200 fluorescence microscope. Both samples were diluted to pico molar concentration and about 200 μL of each solution was deposited on a glass coverslip. A pulsed laser, at 485 nm, 15 μW and 5 MHz, was passed through the objective (PlanApo 63xW, Olympus) and was focused to a diffraction-limited spot. The emission was collected by the same objective and passed through a 100 μm pinhole and a 585/55m filter before being detected on a Single Photon Counting Avalanche Diode. The data was collected by one-time measurement and saved in time-tagged time-resolved format to enable offline calculation of fluorescence bursts, fluorescence lifetime and fluorescence correlation spectroscopy (FCS) using the SymPhoTime software. All figures were produced in OriginPro 8.

2.3 Results and Discussion

2.3.1 *Water Soluble QDs*

The absorption and PL spectra of QDs before and after the ligand exchange reaction with diacetylene (DA) and mercaptopropionic acid (MPA) were obtained before crosslinking process (**Figure 2.1**). All the absorption spectra showed a peak at 580 nm without significant shifts upon ligand exchange, indicating that QDs were not damaged by the ligand exchange reaction and that water-soluble QDs synthesis was successful. There was a unique doublet peak at around 430 nm from QD-DA sample, which is characteristic of the diacetylene moiety.[1] The same concentration of QDs were used for both DA and MPA ligand exchange; however, the product absorption of QD-DA was higher than one of QD-MPA sample, which suggested that DA showed an increased efficiency in exchanging ligands than MPA. This analysis was also supported by visual observation under room light, where a darker yellow color was found for QD-DA sample resulting from a higher concentration of QDs present in the solution (**Figure 2.1 inset**).

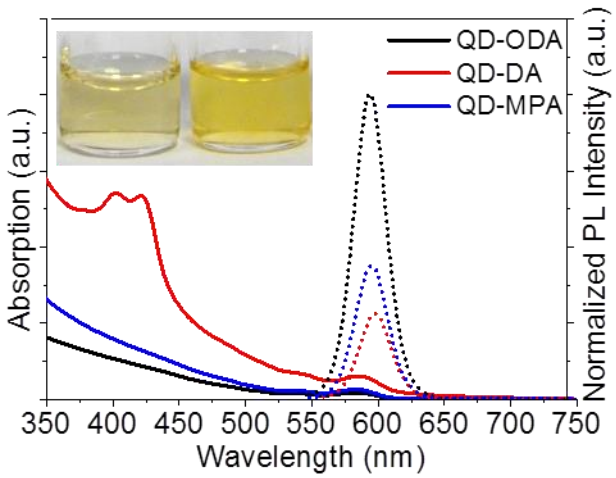

Figure 2.1: Absorption (solid) and photoluminescence (dotted) of QDs before (black) and after the ligand exchange with DA (red) and MPA (blue). Inset is a picture of QDs ligand exchange with DA (right) and MPA (left) under ambient light.

After ligand exchange with either MPA or DA, the emission of QD was quenched compared to the pre-exchanged emission (**Figure 2.1, dotted**), which has been previously observed and explained by the thiol group of the water-solubilizing ligands acting as a stronger quencher than the native octadecylamine ligands.[6, 7] The fact that QD-DA fluorescence decreased more than QD-MPA implied that there were more DA ligands attached to QDs surface. Due to the longer hydrophobic chain of DA, DA can attract each other on the surface via hydrophobic interactions and create a denser packing on the surface of QDs, thereby resulting in better solubility and more complete ligand exchange.

2.3.2 *Photocrosslinking Results*

Crosslinking duration was optimized by monitoring the fluorescence and FT-IR spectra as a function of time. As the QD-DA solution was being exposed to hand-held UV light (254 nm), which initiates DA crosslinking, a small portion of the solution was taken periodically for the analysis. PL of each sample was plotted against UV exposure time (**Figure 2.2 a**). Within 30 minutes of UV exposure, the PL intensity increased, then after 30 minutes the fluorescence gradually decreased until about 150 minutes, at which point there was almost no emission detected from the QDs. Interestingly, we also observed that an increase in PL intensity occurred as some samples were left under the 530 nm excitation beam in the fluorometer, indicating that visible light could also initiate the reaction in a similar manner as UV light. Each connected set of shapes in **Figure 2.2 b** represents the fluorescence intensity of a sample that was taken from the UV-reaction solution at a specific time and measured consecutively under 530 nm excitation, showing the combined effects of UV and visible light illumination. This continuous PL measurement was terminated once the PL intensity stopped increasing. It can be seen that samples with 20, 30, 60, and 100 minutes of UV exposure showed PL enhancement upon

subsequent visible light exposure. However, before 20 minutes of UV photocrosslinking, the visible light seemed no effect on the PL intensity. Based on these observations, 20-30 minutes of UV exposure followed by approximately 15 minutes of visible light crosslinking created the brightest QD-DA samples. However, it was practically not possible to expose more than two samples (QD-DA and QD-MPA) to 530 nm excitation beam simultaneously for subsequent experiments; therefore, the optimal UV exposure period was set to be 30 minutes to compensate the 15 minutes of visible light crosslinking in this research.

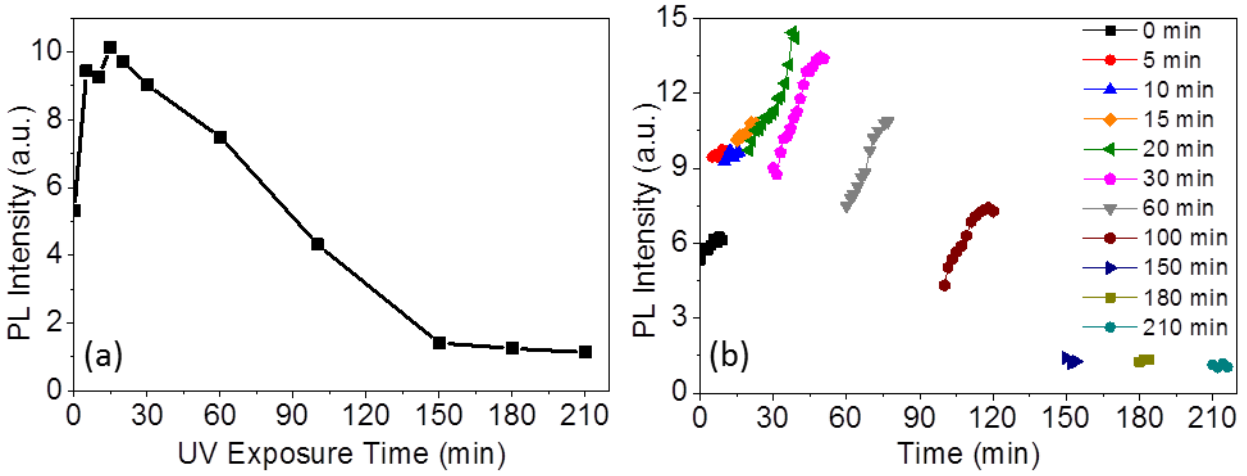

Figure 2.2: (a) Change in fluorescing intensity as a function of UV exposure time. (b) Photoluminescence change observing increase as each sample was irradiated by the 530 nm excitation light in the fluorometer.

In order to further investigate the degree of crosslinking, FT-IR spectra of four samples (taken at 0, 20, 100, and 210 minutes of UV exposure) were obtained (**Figure 2.3**). All four transmittance spectra were normalized at 2922 cm^{-1}, the sp^3 asymmetric C-H stretching, to provide a way to normalize the peaks. This led to no change in the intensity of the 2850 cm^{-1} symmetric C-H stretching peak being observed, as expected since normalizing one of these peaks should automatically normalize the other (**Figure 2.3 a**). In the same region, another peak at 3012 cm^{-1}, typically assigned to C-H stretching of alkene groups, decreased as the sample was

exposed to UV light for longer periods. This peak does not appear in our reaction scheme, suggesting that there could have been incomplete crosslinking due to the absence of adjacent diacetylene to crosslink to leading to C=C groups terminated with C=C–H bonds. **Figure 2.3 b** is an expanded region showing C≡C stretching frequencies between 2100-2300 cm^{-1}. Two peaks were observed: one at 2153 cm^{-1} and the other at 2254 cm^{-1} from the sample before UV exposure, characteristic of stretching of C≡C in a diacetylene motif.[2, 3, 5, 8] After 20 minutes of crosslinking, the peak at 2254 cm^{-1} decreased significantly compared to the one at 2153 cm^{-1}; however, both

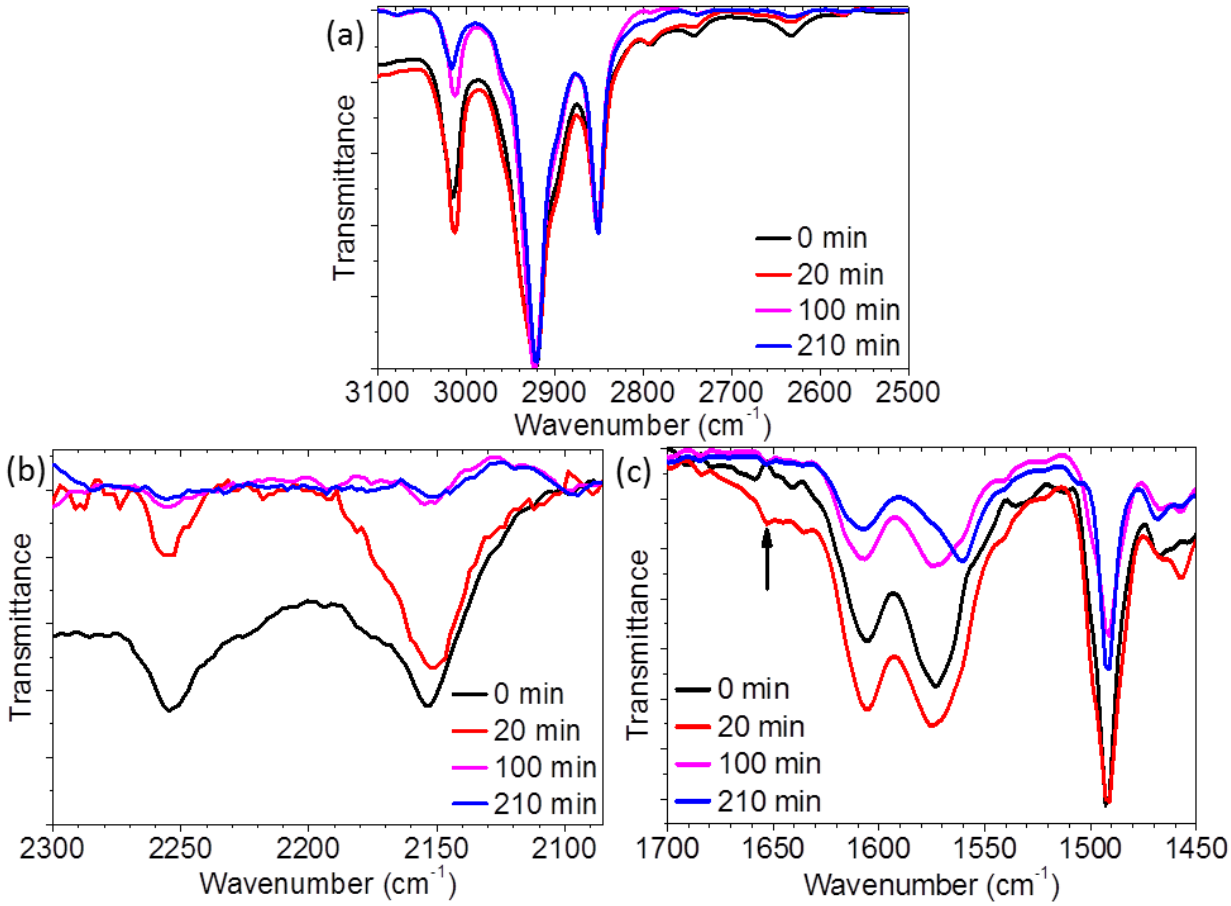

Figure 2.3: FT-IR transmittance of QD-DA before (black) and after 20 minutes (red), 100 minutes (pink), and 210 minutes (blue) of UV (254nm) exposure, separated into three regions; (a) C-H and C=C-H stretching, (b) -C≡C-C≡C- stretching, and (c) unconjugated C=C and C=O stretching.

characteristic diacetylene bands disappeared after 100 minutes of UV exposure. The last FT-IR figure highlights the 1450-1700 cm^{-1} region, which includes C=C bands, resulting from the crosslinking reaction and C=O peaks from the terminal carboxylic groups (**Figure 2.3 c**). The two peaks at 1573 cm^{-1} and 1604 cm^{-1} are assigned as C=O stretches of deprotonated and protonated –COOH, respectively. This assignment agrees with the FT-IR study on ligands containing carboxylic group on the surface of CdTe quantum dots. [9] The intense peak at 1492 cm^{-1} is most likely due to the C-H bending of alkane groups. The decrease in this peak from 20 minutes to 100 minutes sample might indicate a change in the ligand arrangement caused by crosslinking of diacetylene ligands, which weakens the bending mode. The conjugated double bonds formed upon crosslinking is known to show a peak with weak intensity which could be assigned to a small peak at 1652 $cm^{-1,}$, particularly since this peak was not present before UV exposure. However, this assignment is unclear due to possible overlap of several peaks in this region. Overall, there was quite a significant decrease in several peaks in the FT-IR spectra from 20 minutes to 100 minutes of UV exposure, indicating that even though crosslinking occurred over 20 minutes, it degraded within 100 minutes. From this data it can be postulated that, due to limitations in crosslinking, the ligands could be rearranged or dissociated during 20-100 minutes of UV exposure.

2.3.3 *Stability of Diacetylene Capped QDs*

The colloidal stability of UV-exposed (partially-crosslinked) and non-UV exposed (non-crosslinked) diacetylene capped QDs were monitored in water under continuous room light exposure, along with the short MPA water-solubilized QDs as a control; solutions were contained in 4-windowed semi-micro fluorometer cells with a stopper. Fluorescence images under a hand-held UV light (long wave at 366 nm) were captured periodically over an 11-day

period, until the visible difference between the four samples were observed (**Figure 2.4**). Within a day, QD-MPA that was exposed to UV light for 30 minutes showed significant precipitation, and after 5 days all the QDs were aggregated out of water. Similar to this observation, a large amount of non-UV exposed QD-MPA also lost their solubility in water within a few days. This instability was suggested to be due to oxidation of thiol groups binding to the surface of QDs.[10] The UV exposed sample having shorter stability agrees with this explanation; UV exposure accelerated this oxidation process. The colloidal stability in water of both the QD-DA samples (UV-exposed and non-UV exposed) improved significantly compared to QD-MPA samples. Interestingly, the QD-DA without UV exposure showed more stability after 11 days than QD-DA with UV exposure, which showed a gradual decrease in colloidal stability.

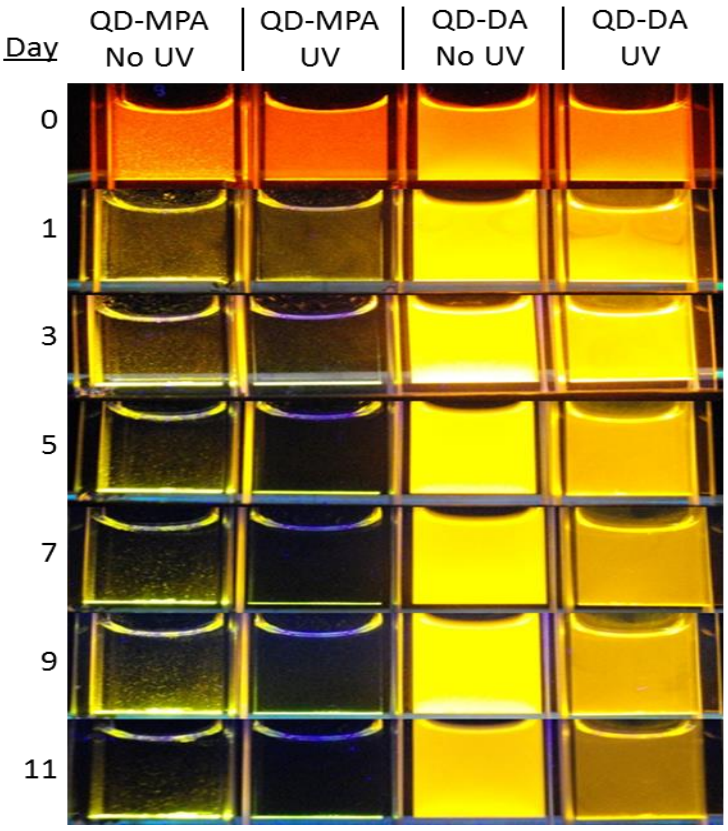

Figure 2.4: Fluorescence of QD-MPA and QD-DA showing the colloidal stability under continuous room light exposure of each sample labeled above. Pictures were taken periodically under hand-held UV lamp (at 366nm).

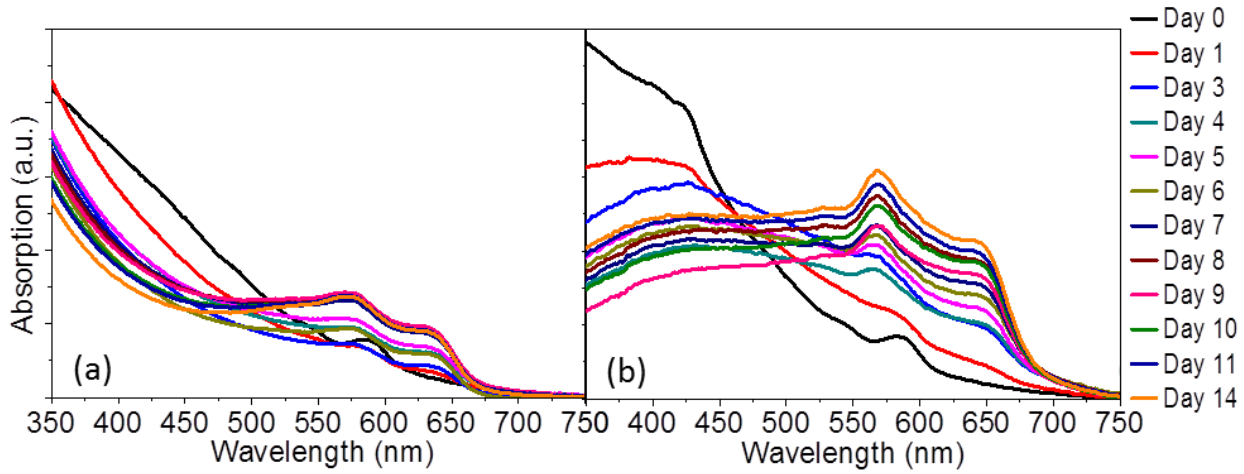

Figure 2.5: Absorption overlays of QD-DA that was (a) exposed and (b) was not exposed to UV light before transferring to water. Absorption was measured periodically for two weeks while both samples were exposed to continuous ambient light.

During this stability test, absorption spectra of QD-DA were also taken, making sure to avoid agitation the solution and ensure aggregates remained precipitated at the bottom of the cells and thus not measured to monitor crosslinking under visible (room) light (**Figure 2.5**). Immediately after the phase transfer to water, the unique feature of diacetylene peak around 400-450 nm region reduced in the UV-exposed (partially-photocrosslinked) QD-DA sample (**Figure 2.5 a, black**), but was still present in the non-UV exposed QDs (**Figure 2.5 b, black**), as would be expected when no crosslinking occurs. As each sample was placed under room light, the difference in the absorption spectra became apparent over time. Both spectra showed a newly formed peak around 650 nm after 24 hours of ambient light exposure. The increase in this peak stops after a week in the UV irradiated QD-DA, but continues to grow in the non-UV exposed sample. The QDs absorptions seem to be blue-shifted in both cases, probably caused by the overlap with crosslinked diacetylene absorption near at 550 nm, indicating formation of the red-absorbing polymer phase.[11] We assign these two peaks (at ~550 nm and ~650 nm) as evidence of crosslinking between DA ligands. The fact that these peaks are not so pronounced after UV

irradiation suggests that UV induced crosslinking can create a competition between crosslinking and desorption of DA ligands from the surface of QDs leading to only a small number of crosslinkages in each QD. This results in the reduction of the diacetylene peak at 400-450 nm region. Even without UV exposure, there were increases in the crosslinked DA absorptions, which indicates crosslinking between the DA ligands that remained on the QD are facilitated by visible-light. This visible-light is mediated by QDs since the QDs used here absorb 580 nm room visible light and emits at 600 nm (**Figure 2.1**), and also the absorption spectra of QD-DA without UV exposure showed absorption peaks from 550-650 nm (**Figure 2.5**). Therefore, individual DA ligands on the surface of QDs were crosslinked to each other after the QDs absorbed the visible-light, and presumably resulted in electron transfer between the QD and the DA ligand to initiate crosslinking. This idea is consistent with the photoluminescence discussion earlier. Together with the fluorescence observation, UV-catalyzed crosslinking could result in higher chance of photooxization which removes the diacetylene and reducing the colloidal stability; whereas, the visible light initiated crosslinking can maximize the crosslinking of DA ligands without losing ligands and leads to an increased coverage on the surface of QDs and better stability in water.

3.2.4 *Fluorescence Correlation Spectrophotometry (FCS)*

Single molecule fluorescence spectroscopy analysis of UV-exposed and non-UV exposed QD-DA samples revealed more insights into the aggregation formation after the 14-day period of constant ambient light exposure. **Figure 2F a and b** show burst integrated fluorescence traces of UV exposed and non-UV exposed QD-DA, respectively. The UV exposed sample shows broader peaks with high intensity whereas the non-UV exposed sample showed less intense and narrower peaks. The peaks in the traces correspond to fluorescing QDs diffusing through the

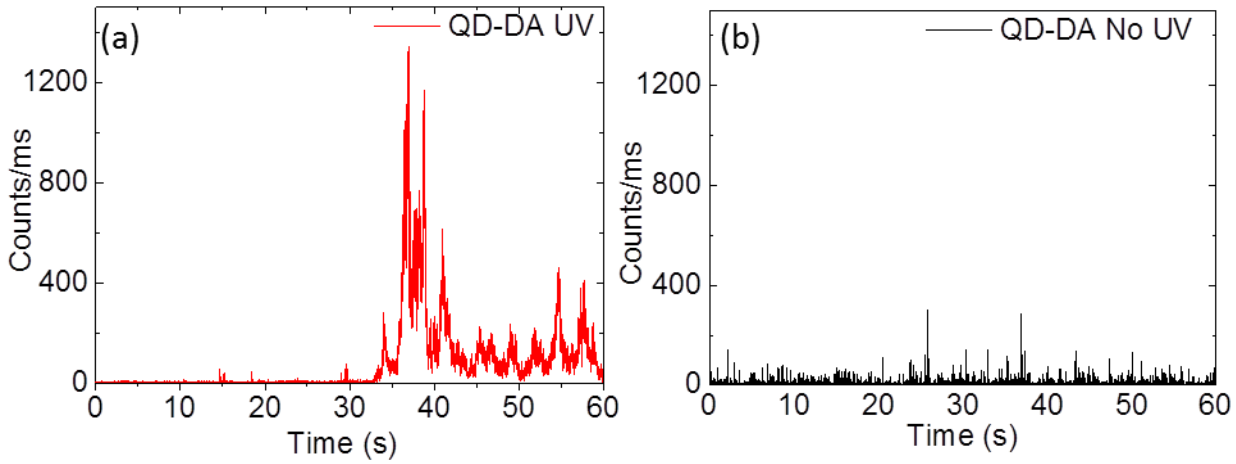

Figure 2.6: Fluorescence burst traces of QD-DA that were (a) crosslinked by UV exposure and (b) not exposed to UV light. The data was taken after 14 days of stability test under non-stop room light exposure.

focused diffraction-limited laser focus. When large and highly fluorescing particles diffuse through the laser focus, the peaks are wide and intense due to multiple QDs contributing to the fluorescence intensity and the lower diffusion constants of the larger aggregates. Therefore, **Figure 2.6 a** indicates the presence of larger, bright QD aggregates. In order to quantitatively analyze these samples, the average diffusion times of QD-DA particles were computed by converting the intensity fluctuation into autocorrelation functions (ACF, *G(τ)*) (**Figure 2.7 a**).

It is necessary to consider the contribution of QD blinking when fitting to ACF; therefore, the following equation is employed,[12]

$$G(\tau) = G_{\text{diff}}(\tau) \cdot \left(1 + \frac{F \times A\tau^{\alpha-2}}{1-F}\right) \quad \textbf{(2.1)}$$

where

$$G_{\text{diff}}(\tau) = G(0) \cdot \frac{1}{\left(1+\frac{\tau}{\tau_D}\right)} \cdot \frac{1}{\sqrt{1+\left(\frac{w_0}{z_0}\right)^2 \cdot \frac{\tau}{\tau_D}}} \quad \textbf{(2.2)}$$

The individual parameters in the above equation are denoted as follows[12-15]:

τ: the lag time

F: the fraction of quantum dots with detectable fluctuations

A: proportionality factor (scaling coefficient)

α: the power-law exponent

G(0): the autocorrelation amplitude at zero-time

τ_D: the lateral diffusion time

w_0: width of the focus beam

z_0: depth of the focus beam

w_0 and z_0 set to be 500 nm and 2 μm, respectively, which have been suggested previously.[14] By setting $F = 0$ or allowing it to be fit, the possibility of non-blinking (from aggregates) and blinking (from single QDs) to be explored. The UV exposed sample showed a nearly perfect fit to the non-blinking situation (**red curve in Figure 2.7 a**), which can be expected since the QD-DA UV sample contains aggregates with multiple QDs stuck together, statistically eliminating the observation of blinking, since these events are not synchronized.[12] On the other hand, the QD-DA sample without UV exposure showed a better fit to the blinking autocorrelation functions at the shorter lag time (**thick black curve**) than to the non-blinking function (**thin gray curve**).

This result indicated that the non-UV exposed sample remained as single particles even after 14 days under ambient light exposure. From these fits, the diffusion time for UV exposed and non-UV exposed samples were calculated to be 265 ± 5 ms and 3.09 ± 0.11 ms, respectively. The diffusion time under our experimental set-up (one-photon excitation) is defined as:

$$\tau_D = \frac{{w_0}^2}{4D} \qquad \textbf{(2.3)}$$

where *D* is the diffusion coefficient.[13, 15] Using this equation, the diffusion constants were translated to be 20 ± 1 $\mu m^2/s$ for non-UV and 0.236 ± 0.004 $\mu m^2/s$ for UV exposed QD-DA.

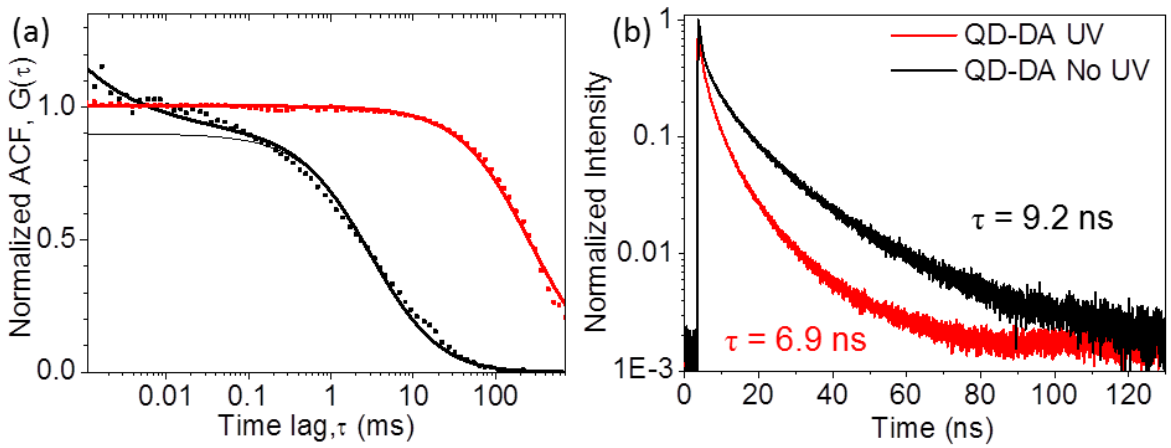

Figure 2.7: (a) ACF plots of QD-DA UV (red) and No UV (black). The best ACF fits are shown in thick curves: with blinking effect for QD-DA No UV (black) and without blinking effect for QD-DA UV (red). For QD-DA No UV, the thin gray curve is showing ACF fits without blinking effects. (b) Lifetime traces with corresponding lifetime: QD-DA UV in red and QD-DA No UV in black.

These values can be further converted into hydrodynamic diameters using the Stokes-Einstein relation.[16, 17]

$$D = \frac{kT}{4\pi\eta r} \qquad (\mathbf{2.4})$$

where k is the Boltzmann constant, T is the absolute temperature, η is a viscosity of a medium, and r is hydrodynamic radius. Using a temperature of 20 C^{o} in the water medium[16], the hydrodynamic radius were found to be 10 nm for non-UV and 900 nm for UV exposed QD-DA. The hydrodynamic radius for a single water solubilized red emitting CdSe/ZnS being around 10 nm has been reported[18, 19], which further supports that the non-UV exposed sample remained as single particles and exhibited excellent colloidal stability over 2 weeks. The hydrodynamic radius of QD-DA UV being 900 nm is clear evidence of aggregation formed in the UV exposed sample. Furthermore, the fluorescence lifetime of both samples were measured and calculated to be 9.2 ns and 6.2 ns for QD-DA without and with UV exposure, respectively (**Figure 2.7 b**). The shorter fluorescence lifetime is known to be an indicative of fluorescing quenching caused by

aggregation. All the single molecule spectroscopy results suggest that the UV-exposed sample resulted in lower colloidal stability and the formation of aggregation whereas the non-UV exposed sample showed significantly improved colloidal stability in water and remained as single particles. This supports the earlier discussion that UV exposure could trigger the photooxidation of thiol groups at the surface of QDs, causing the diacetylene ligands to dissociate and lead to lower stability. The non-UV exposed diacetylene can crosslink by the visible-light QD-mediated-photocatalysis, which enhanced colloidal stability in water.

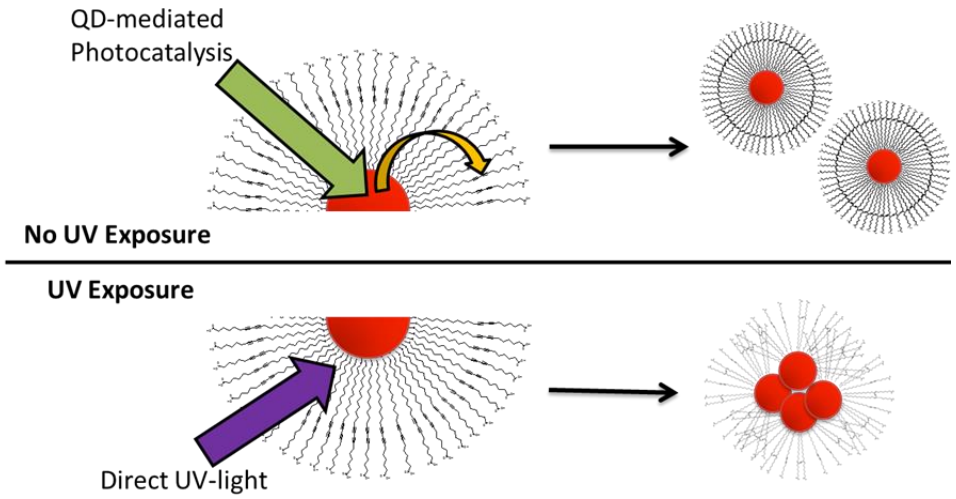

Figure 2.8: Scheme illustrating the difference in colloidal stability results from different phorocrosslinking of DA ligands

2.4 Conclusion

The synthesis of enhanced colloidal stability of water-soluble QDs was developed by capping QDs with photocrosslinking diacetylene ligands through either UV-light or QD-mediated visible-light photocatalysis. QD-DA exhibited higher colloidal stability than the QD-MPA control. During the stability examination, the slow formation of crosslinking between DA ligands in non-UV exposed sample was observed in periodic absorption measurements, which

resulted in higher colloidal stability over time than QD-DA that had been exposed to UV light (**Figure 2.8**). After two weeks of the stability test, the product solutions of QD-DA with and without UV exposure were analyzed by FCS. The results confirmed that the UV exposed QD-DA showed a slower diffusion time and a larger hydrodynamic radius, indicating the formation of aggregates. We suspect that the formation of aggregation is due to the UV exposure which photooxidized and desorbed the ligands from the surface of QDs. On the other hand, the non-UV exposed QD-DA remained as single particles since oxidation of thiol group was not initiated but still crosslinked through QDs mediated visible-light. Therefore, we have developed a method in which the QDs help to crosslink the ligands, which in turn help to stabilize those same QDs and have thus termed this as a 'symbiotic approach' to QD-ligand chemistry.

2.5 References

1. Viguerase-Santiago, E.; Hernandez-Lopez, S.; Rodroguez-Romero, A., Photochemical cross-linking study of polymers containing diacetylene group in their main chain and azobenzene compounds as pendant group. *Superficies y Vacio* 2006, 19, 7.

2. Roman, M.; Baranska, M., Vibrational and theoretical study of selected diacetylenes. *Spectrochimica Acta Part a-Molecular and Biomolecular Spectroscopy* 2013, 115, 493-503.

3. Kim, T.; Ye, Q.; Sun, L.; Chan, K. C.; Crooks, R. M., Polymeric self-assembled monolayers .5. Synthesis and characterization of omega-functionalized, self-assembled diacetylenic and polydiacetylenic monolayers. *Langmuir* 1996, 12, 6065-6073.

4. Kim, T. S.; Crooks, R. M.; Tsen, M.; Sun, L., Polymeric Self-Assembled Mnolayers. 2. Synthesis and Characterization of Self-Assembled Polydiacetylene Monolayers and Multilayers. *Journal of the American Chemical Society* 1995, 117, 3963-3967.

5. Khlifi, M.; Paillous, P.; Delpech, C.; Nishio, M.; Bruston, P.; Raulin, F., ABSOLUTE IR BAND INTENSITIES OF DIACETYLENE IN THE 250-4300 CM(-1) REGION - IMPLICATIONS FOR TITAN ATMOSPHERE. *Journal of Molecular Spectroscopy* 1995, 174, 116-122.

6. Uyeda, H. T.; Medintz, I. L.; Jaiswal, J. K.; Simon, S. M.; Mattoussi, H., Synthesis of compact multidentate ligands to prepare stable hydrophilic quantum dot fluorophores. *Journal of the American Chemical Society* 2005, 127, 3870-3878.

7. Breus, V. V.; Heyes, C. D.; Nienhaus, G. U., Quenching of CdSe-ZnS Core-Shell Quantum Dot Luminescence by Water-Soluble Thiolated Ligands. *Journal of Physical Chemistry C* 2007, 111, 18589-18594.

8. Kim, T. S.; Crooks, R. M.; Tsen, M.; Sun, L., POLYMERIC SELF-ASSEMBLED MONOLAYERS .2. SYNTHESIS AND CHARACTERIZATION OF SELF-ASSEMBLED POLYDIACETYLENE MONOLAYERS AND MULTILAYERS. *Journal of the American Chemical Society* 1995, 117, 3963-3967.

9. Omogo, B.; Aldana, J. F.; Heyes, C. D., Radiative and Nonradiative Lifetime Engineering of Quantum Dots in Multiple Solvents by Surface Atom Stoichiometry and Ligands. *J. Phys. Chem. C* 2013, 117, 2317-2327.

10. Aldana, J.; Wang, Y. A.; Peng, X., Photochemical Instability of CdSe Nanocrystals Coated by Hydrophilic Thiols. *J. Am. Chem. Soc.* 2001, 123, 8844-8850.

11. Alloisio, M.; Demartini, A.; Cuniberti, C.; Muniz-Miranda, M.; Giorgetti, E.; Giusti, A.; Dellepiane, G., Photopolymerization of diacetylene-capped gold nanoparticles. *Physical Chemistry Chemical Physics* 2008, 10, 2214-2220.

12. Heuff, R. F.; Swift, J. L.; Cramb, D. T., Fluorescence correlation spectroscopy using quantum dots: advances, challenges and opportunities. *Physical Chemistry Chemical Physics* 2007, 9, 1870-1880.

13. Schwille, P.; Haustein, E. Fluorescence Correlation Spectroscopy An Introduction to its Concepts and Applications 2006, p. 1-33.

14. Heyes, C. D.; Kobitski, A. Y.; Breus, V. V.; Nienhaus, G. U., Effect of the shell on the blinking statistics of core-shell quantum dots: A single-particle fluorescence study. *Physical Review B* 2007, 75, 8.

15. Murcia, M. J.; Shaw, D. L.; Long, E. C.; Naumann, C. A., Fluorescence correlation spectroscopy of CdSe/ZnS quantum dot optical bioimaging probes with ultra-thin biocompatible coatings. *Optics Communications* 2008, 281, 1771-1780.

16. Krynicki, K.; Green, C. D.; Sawyer, D. W., Pressure and Temperature-Dependence of Self-Diffusion in Water. *Faraday Discussions* 1978, 66, 199-208.

17. Edward, J. T., Molecular volumes and the Stokes-Einstein equation. *Journal of Chemical Education* 1970, 47, 261.

18. Callan, J. F.; Raymo, F. i. M.; ebrary Inc., Quantum dot sensors technology and commercial applications. Pan Stanford Pub.,: Singapore, 2013; p. 1 online resource.

19. Kirchner, C.; Liedl, T.; Kudera, S.; Pellegrino, T.; Javier, A. M.; Gaub, H. E.; Stolzle, S.; Fertig, N.; Parak, W. J., Cytotoxicity of colloidal CdSe and CdSe/ZnS nanoparticles. *Nano Letters* 2005, 5, 331-338.

Chapter 3:

Are Bidentate Ligands Really Better Than Monodentate Ligands For Nanoparticles?

Hiroko Takeuchi, Benard Omogo and Colin D Heyes*.

Department of Chemistry and Biochemistry, University of Arkansas, 345 N Campus Drive, Fayetteville, AR 72701.

**to whom correspondence should be addressed: cheyes@uark.edu*

Abstract

Coordinating ligands are widely used to vary the solubility and reactivity of nanoparticles for subsequent bioconjugation. Although long-term colloidal stability is enhanced by using bidentate coordinating ligands over monodentate ones, other properties such as nonspecific adsorption of target molecules and ligand exchange have not been quantified. In this study, we modified a near- infrared dye to serve as a highly sensitive reporter for nonspecific binding of thiolated target molecules to nanoparticle surfaces that are functionalized with monodentate or bidentate coordinated ligands. Specifically, we analyzed nonspecific binding mechanisms to quantum dots (QDs) by fitting the adsorption profiles to the Hill equation and the parameters are used to provide a microscopic picture of how ligand density and lability control nonspecific adsorption. Surprisingly, bidentate ligands are worse at inhibiting adsorption to QD surfaces at low target/QD ratios, although they become better as the ratio increases, but only if the nanoparticle surface area is large enough to overcome steric effects. This result highlights that a balance between ligand density and lability depends on the dentate nature of the ligands and controls how molecules in solution can coordinate to the nanoparticle surface. These results will have major implications for a range of applications in nanobiomedicine, bioconjugation, single molecule spectroscopy, self-assembly and nano(photo)catalysis where both nonspecific and specific surface interactions play important roles. As an example, we tested the ability of monodentate and bidentate functionalized nanoparticles to resist nonspecific adsorption of IgG antibodies that contained free thiol groups at a 1:1 QD:IgG ratio and found that QDs with monodentate ligands did indeed result in lower nonspecific adsorption.

Keywords: *Non-specific binding, biocompatible nanoparticles, quantum dots, ligand exchange, surface chemistry, protein labeling*

A range of ligands to render nanoparticles water-soluble and biocompatible have been developed over recent years, which has led to significant extension of their applications, particularly for colloidal quantum dots (QDs) as fluorescent labels in biophysics and molecular biology.[1-3] The two most common formulations to render QDs water-soluble involve using coordinating thiolated ligands[1, 4-6] or amphiphilic polymers,[7-9] although other methods have also been reported.[10-12] There are advantages and disadvantages to each method and have been extensively discussed in the literature.[13, 14] The primary advantages of polymer-functionalized QDs are their long-term colloidal stability and reduced effects of the environment on their optical properties,[15] while thiol-functionalized QDs are usually cheaper and easier to make, require less workup and, most importantly, result in a smaller colloidal size.[16] This latter property makes ligand-exchanged QDs attractive platforms for advanced biolabeling applications where probe size is a critical issue.

One difficulty in using coordinating ligands is that they can be labile or exchanged with other molecules that coordinate to the QD surface leading to both heterogeneous attachment of biomolecules as well as eventual aggregation of the QDs.[4, 6] Using thiolated ligands with bidentate or multidentatate as opposed to monodentate thiol functionality has been shown to improve the colloidal stability,[17-19] but other important properties such as nonspecific surface adsorption of target molecules have not been as well-studied. Of particular importance is the adsorption of thiol groups to the nanoparticle surface, since cysteine residues are primary targets used for site-specific fluorescence labeling of biomolecules,[20, 21] but the same reactive group is also the coordinating groups that are used in the water-solubilizing ligands. In this report, we modified a near-infrared dye to serve as a highly-sensitive reporter for non-specific adsorption of thiols to nanoparticle surfaces. Monodentate (mercaptopropanoic acid, MPA) and bidentate (dihydrolipoic acid, DHLA) functionalized QDs are used to investigate the effect of ligand coordination

configuration on non-specific adsorption of thiols. We performed these experiments with two core-shell QDs that have the same optical properties but with different shell thicknesses to investigate the effects of particle surface area.

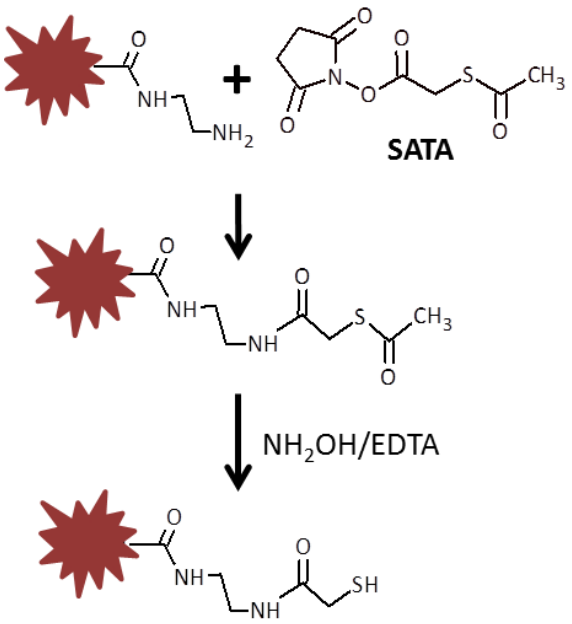

Figure 3.1: Reaction scheme for modifying amine functionalized dyes to convert to thiolated dyes by using SATA.

A commercially available amino-functionalized near-infrared dye, Atto 700 amine (Atto-Tec GMBH, Germany), was converted to a thiolated dye (dye-SH) by reaction with SATA (*N*-Succinimidyl S-Acetylthioaccetate, Pierce, Thermo, Rockford, IL) (**Figure 3.1**). A 0.304 mmol of the amine dye was added to SATA (in 1:20 and 1:100 molar ratios) in 1.5 mL phosphate buffered saline (PBS, Amresco Solon, OH) at pH 7.2, and left to react for 30 minutes. The reaction was monitored by reverse-phase HPLC (Shimadzu Prominence, Kyoto, Japan) on a Supelco Discovery C-18 column (Sigma Aldrich, St. Louis, MO) and MALDI-TOF mass spectrometry (Bruker UltraflexII, Billerica, MA). In **Figure 3.2**, we show the HPLC traces for

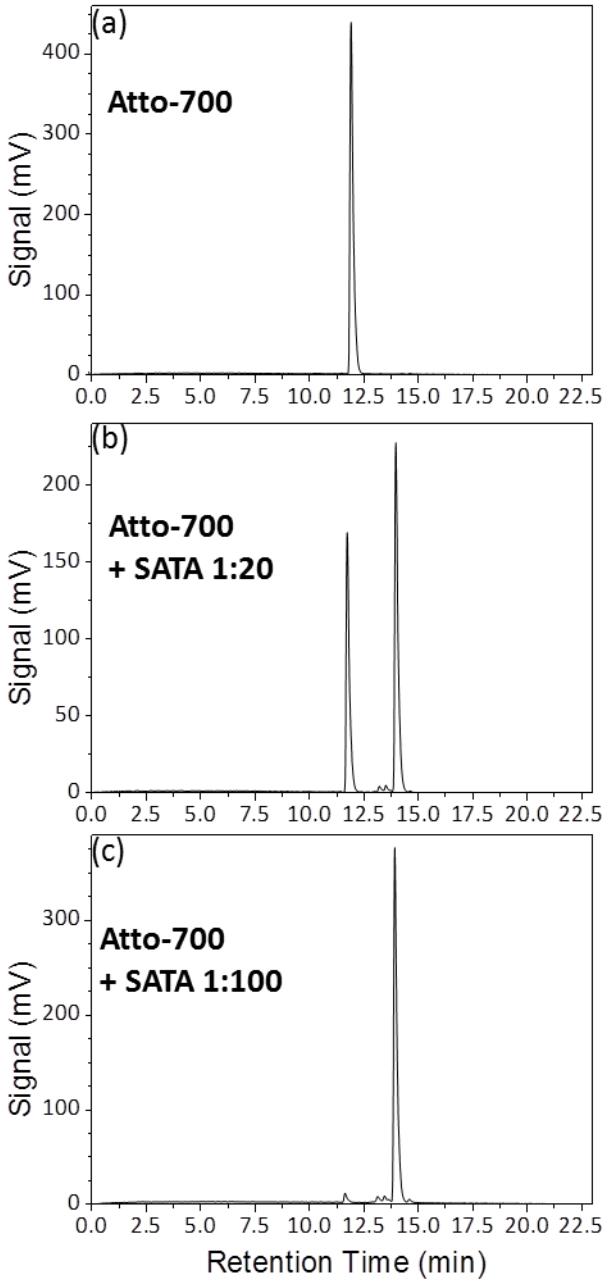

Figure 3.2: HPLC chromatograms of the unmodified (amino-functionalized) and modified (thioester functionalized) Atto700 dye.

Atto 700 before and after the reaction with SATA. The more polar amino-dye (Atto700-NH_2) elutes from the column sooner than the less polar protected thiol (Atto700-S-$COCH_3$). Mass spectra of the reactant and product are shown in the Supporting Information. It was found that a molar ratio of 1:100 (dye:SATA) was required to completely convert Atto700 into the protected

thiol; the reaction has only ~55% yield at a 1:20 ratio (the ratio recommended by the manufacturer). The dyes were stored in protected form and deprotected immediately prior to use to limit disulfide bond formation in solution. Deprotection of the thioester was performed by reaction with hydroxylamine and ethylenediaminetetraacetic acid (EDTA, EMD Philadelpha, PA) at pH 7.4 followed by evaporation under reduced pressure, as recommended by the manufacturer. Atto 700 was chosen as the model dye ligand to monitor the nonspecific adsorption and/or exchange of thiolated molecules to QD surfaces for two primary reasons: first, it absorbs at much lower energy than the QD so that the dye spectrum can be easily separated from the QD spectrum, and second, it is a highly water-soluble, zwitterionic dye, which should reduce electrostatic interactions between the molecule and QD surface[5] to focus on the thiol coordination chemistry. The ligands on the QD are as short as possible relative to the length of the linker between the thiol and the dye to minimize steric hindrance imposed by the ligand layer so that the thiol adsorption processes can be more easily quantified.

Octadecylamine (ODA)-coated CdSe/ZnS quantum dots were purchased from NN-Labs (Fayetteville, AR) and dissolved in toluene. The absorption wavelength of the excitonic peak was 520 nm (see Supporting Information), corresponding to a core diameter of 2.5 nm. Transmission electron microscopy (TEM) images of the thin-shell and thick-shell QD samples (**Figure 3.3 a and b**, respectively) were obtained on an FEI TECNAI 200kV electron microscope (Hillsboro, OR) to obtain their overall size and size distribution (**Figure 3.3 c**). Using the first exciton peak position of the absorption spectra to estimate core size, and the TEM images to determine overall size, the shell thickness for each sample was found to be ~3 and ~7 monolayers (ML) respectively.

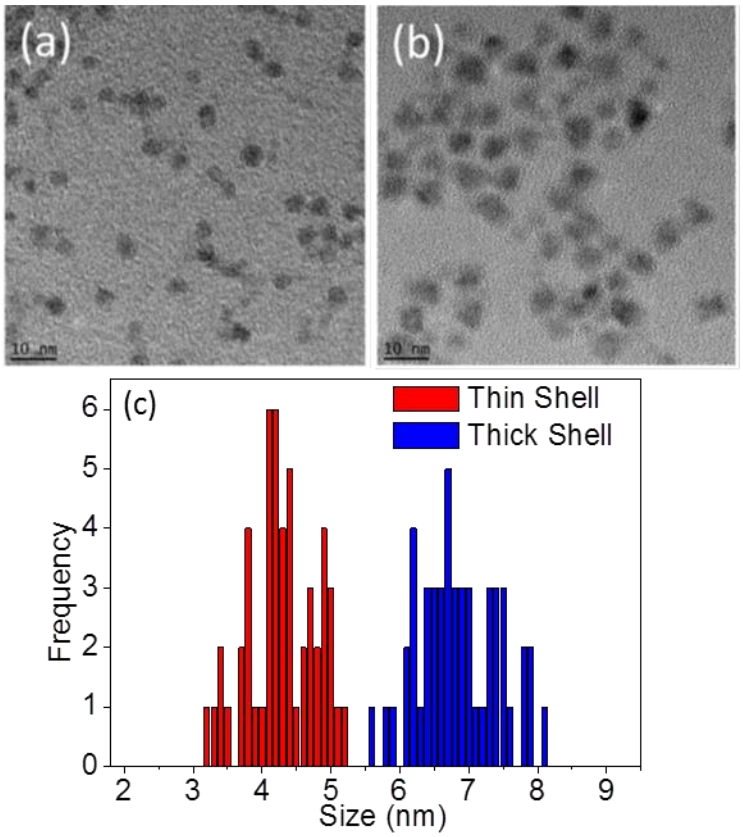

Figure 3.3: TEM images of (a) thin shell and (b) thick shell QDs and (c) their size histograms.

The native ODA ligands were exchanged with mercaptopropanoic acid (MPA, Alfa Aesar, Ward Hill, MA), or dihydrolipoic acid (DHLA), which had been reduced from DL-α-lipoic acid (TCI, Portland, OR) by reaction with $NaBH_4$ (Alfa Aesar) and $NaHCO_3$ (EMD),[17] using a general ligand exchange procedure.[22] Briefly, ODA-QDs were precipitated from toluene by the addition of acetone (VWR), centrifuged at 1900g (4000rpm on a Clinical 50 centrifuge, VWR) and the supernatant discarded. DHLA or MPA was dissolved in methanol, and the solution adjusted to pH 10 by the addition of tetramethylammonium hydroxide pentahydrate (Alfa Aesar). The concentration of QDs was determined from the size-dependent extinction coefficients at the band edge.[23] A molar ratio of $1:3\times10^5$ QD:ligand was used for the ligand exchange to ensure as complete a ligand exchange as possible under reproducible conditions. The ligand solution was added to the precipitated QDs and stirred under reflux for 3 h under

argon. Then, the QD-methanol solution was precipitated with a mixture of ethyl acetate and acetone, centrifuged and dissolved in 10 mM phosphate buffer made using Millipore (18.2 MΩ.cm) water. Since the molar ratio of ligand to QD used was in such a huge excess and allowed to exchange for 3 h at elevated temperatures, this results in the ligand exchange being taken to its thermodynamic equilibrium; performing the process overnight did not improve the ligand exchange. Absorption and photoluminescence (PL) spectra of the QDs with thin and thick ZnS shells before and after successful ligand exchanges are shown in the Supporting Information. There is a decrease in the PL upon ligand exchange, with MPA showing a stronger decrease than DHLA. Using a thicker shell resulted in less of a decrease in PL than the thin shell. We used several batches of thin-shell QDs, all with the same specifications (2.5 nm core size, 3 ML of ZnS shell), as well as a batch with the same core, but a thicker shell (7 ML). For some batches of thin-shell QDs, it was observed that upon ligand exchange, significant deep trap state emission was evident in the PL spectra (Supporting Information), suggesting variations in the quality of the ZnS from batch to batch, and highlights the need for thorough QD characterization prior to their use. We did not use the QDs that showed trap emission for any further experiments here.

Non-specific adsorption of thiolated dye molecules onto the monodentate or bidentate-coordinated QDs was studied by exposing the QDs to the dye at QD:dye molar ratios varying from 1:0 to 1:100 in 10 mM PBS buffer at pH 7.2, consistent with typical bioconjugation conditions. After 2 h, the unreacted dyes were separated from the QD-dye conjugates using size-exclusion chromatography (PD-10 Column, GE Healthcare), which showed excellent separation (see Supporting Information) allowing pure QD-dye conjugates to be obtained for quantitative

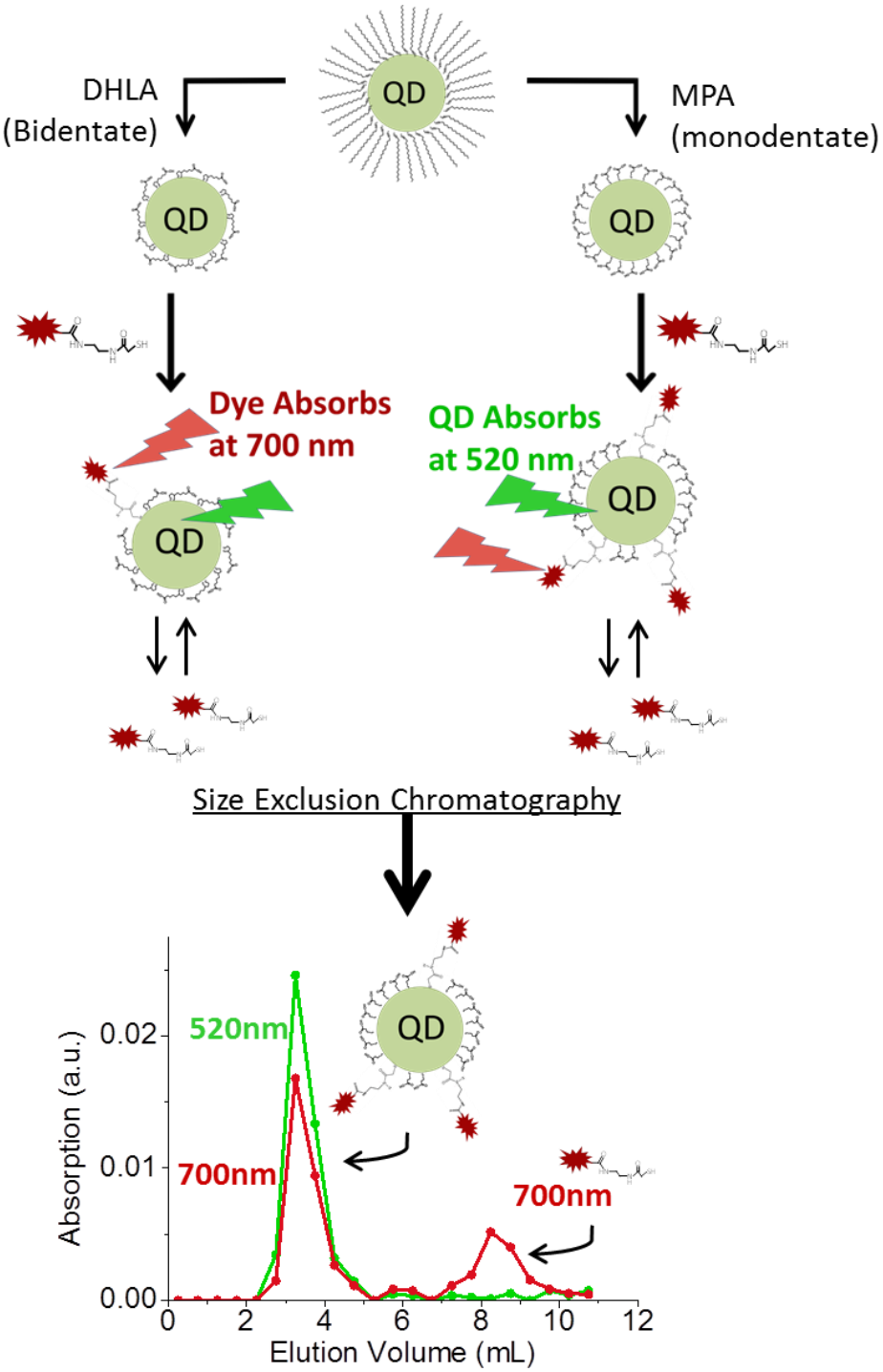

Figure 3.4: Schematic representation of the ligand exchange of octadecylamine (ODA) QDs with monodentate (MPA) and bidentate (DHLA) ligands and the non-specific binding assay of the thiolated dye to each QD surface, followed by separation of unbound dye from the QD-dye conjugates by size exclusion chromatography. The QD-dye conjugates were eluted from the column within 2-4 mL while the free dye was only eluted after 7 mL.

analysis. The conjugates were analyzed by immediately measuring the absorption spectra using a Hitachi 3900H spectrophotometer after separation. Bidentate ligands such as DHLA, which are more strongly attached to the QD,[17, 24] were expected to show lower affinity for the monodentate thiolated dyes compared to the monodentate MPA-QDs at a given ratio of QD:dye. **Figure 3.4** shows a schematic representation of the ligand exchange and thiolated dye reactions as well as the separation of QD-dye conjugates from unbound dye using size exclusion chromatography, which is measured using the absorption of the QD at 520 nm and the Atto 700 dye at 700 nm.

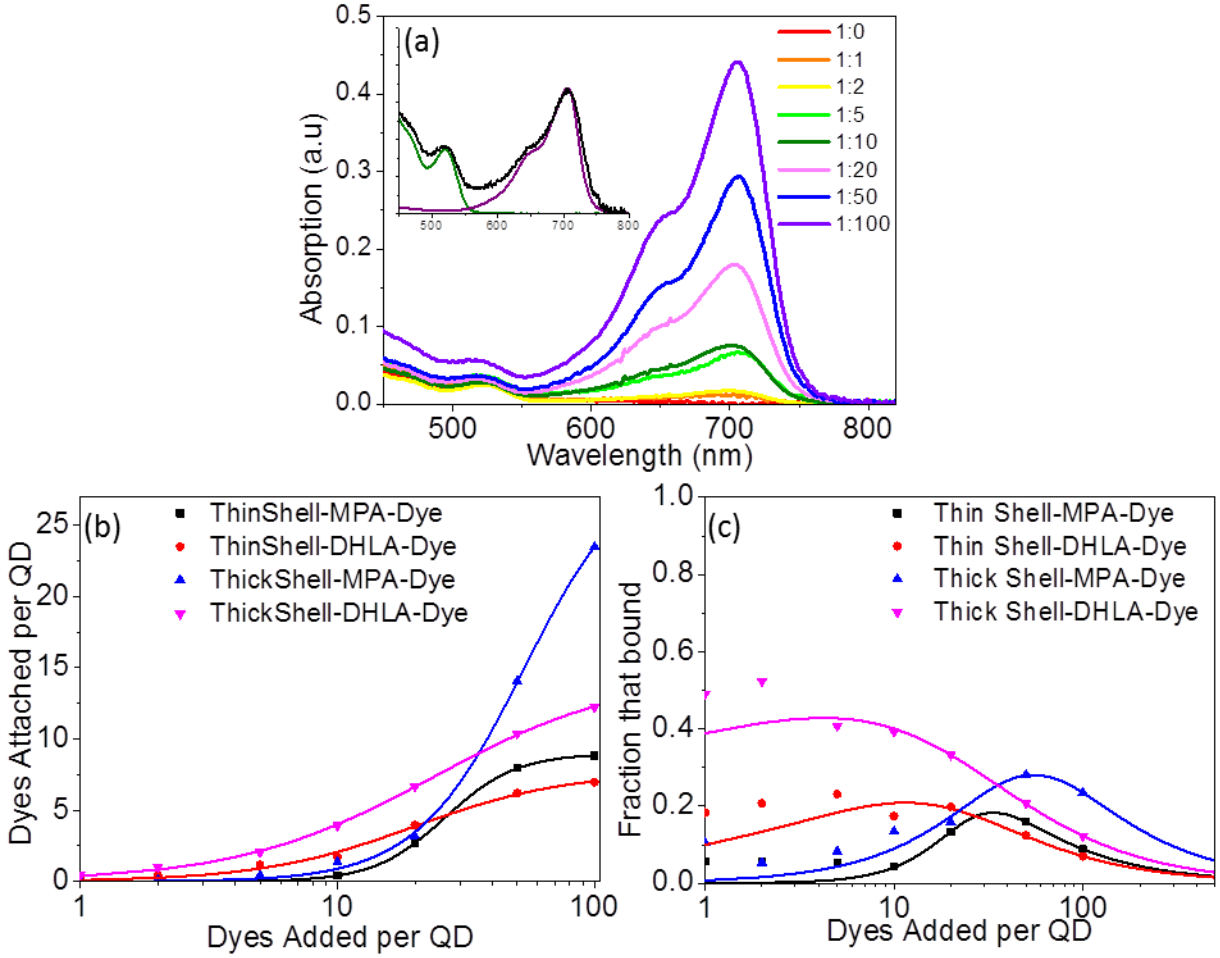

Figure 3.5: (a) Absorption spectra of QD-dye conjugates after separation of the unbound dyes by size-exclusion chromatography. (b) Ratio of dyes bound to each QD as a function of the ratio added to the solution together with fits to the Hill equation. (c) Plot of the fraction of dyes added to the solution that was found to bind to each QD sample.

Figure 3.5 a shows the absorption spectra of the QD-Atto 700 conjugates after separation. It is clear that there is an increase in the dye absorption relative to the QD absorption for higher QD:dye ratios, as would be expected. For Atto700, the absorption spectra of the QD and the dye have very little overlap, and they can be easily deconvoluted to provide the concentration of each species (**Figure 3.5 a** inset). A small correction is needed for the absorbance of the dye at the QD λ_{max} in order to accurately measure the QD concentration. There is a small broadening and shifting of the spectrum of the dye following conjugation, but is small enough to not affect the results. The absorption of the dye relative to the QD allows the number of dyes per QD to be calculated as a function of the ratio initially mixed together. In order to calculate the QD/dye ratio, we used the QD extinction coefficients reported by Yu and Peng,[23] although others have also been reported.[25-27] While the exact ratio of QD:dye will depend on which absorption coefficient is used, as long as the same value is consistently used for all samples the observed trends will be the same. **Figure 3.5 b** shows the relationship between the molar excess of dyes added to the QD and the number of dyes that actually bound for thin-shell and thick-shell QDs, each functionalized with either MPA or DHLA. The data were fit to the Hill equation as follows:

$$y = \frac{L_{max} \cdot x^n}{K^n + x^n} \quad (\mathbf{3.1})$$

The excellent fit to the data allowed us to determine the maximum number of dye ligands that can bind, L_{max}, relative binding strength, K, and the Hill coefficients, n, which are listed in **Table 3.1**. **Figure 3.5 b** and **Table 3.1** suggest that the effects of both the ligand coordination geometry and the QD surface area were significant. For thin-shell (lower surface area) QDs, there is surprisingly very little difference of the total number of thiolated dyes that can bind per QD between the MPA-QDs and the DHLA-QDs, saturating at about 8-9 dyes/QD. For thick-shell QDs, this difference is much larger, with MPA-QDs showing a maximum of ~30 dyes/QD

while DHLA-QDs bind about half as many, ~15. There are also differences in the binding strengths with MPA-QDs having higher K values (lower affinities) than the equivalent DHLA-QDs, opposite to our original hypothesis. The Hill coefficients for DHLA-QDs are lower than for MPA-QDs, suggesting mechanistic differences in the binding to MPA-QDs and DHLA-QDs. **Figure 3.5 c** shows the average fraction of added dyes that bound to each QD, together with the Hill equation fits, providing an alternative view of the data in terms of a binding probability, with the mechanistic differences depending on ligand coordination geometry becoming more evident. The fits of probability are calculated using the Hill equation parameters in **Table 3.1** to compute the number of dyes attached as a function of the number of dyes added (varying from 0 to 500) and determining the bound/added fraction. It can be seen that the shapes of the curves in **Figure 3.5 c** depend on the ligand coordination geometry but not on the QD size, and highlights the important role of the thiol coordination for the probability of the thiol to adsorb on the QD surface. The highest probability of binding occurs at low dye:QD ratios for DHLA-QDs while for MPA-QDs, the highest probability is at much higher dye:QD ratios.

	L_{max}	K	n
thin-shell-MPA	8.97 ± 0.15	26.21 ± 0.73	3.14 ± 0.20
thin-shell-DHLA	7.70 ± 0.48	19.85 ± 2.66	1.45 ± 0.18
thick-shell-MPA	29.70 ± 1.37	52.89 ± 3.08	2.08 ± 0.13
thick-shell-DHLA	14.65 ± 0.49	23.55 ± 1.85	1.14 ± 0.05

Table 3.1: Parameters of thiolated dyes binding to QDs from fitting to the Hill equation

Figure 3.5 showed that the maximum number of thiolated dyes that can bind to QDs (L_{max}) only becomes significantly different between monodentate- and bidentate-functionalized QDs for larger surface area QDs. For DHLA-QDs, the *K* values and the Hill coefficients, *n*, are similar whether small or large QDs are used, while they are different for MPA-QDs. It has been discussed that, as the number of potential binding sites increases, the Hill coefficient increases above 1 for both sequential and independent binding mechanisms, and whether the binding shows positive, negative or no cooperativity.[28] Comparing L_{max} to *n* allows us to postulate the possible mechanistic differences in thiols binding to DHLA-QDs compared to MPA-QDs. *n* approaches L_{max} only when the binding is sequential and there is high positive cooperativity. For example, it was found that for 10 binding sites, *n* never exceeds 2.1 for sequential binding or 1.4 for independent binding when there is no cooperativity, and is even less when there is negative cooperativity.[28] It must also be noted that when L_{max} is larger than about 6 and the binding is independent, even positive cooperative binding shows a Hill coefficient less than 2 and decreases weakly with the number of binding sites. For MPA-QDs, $n = 3.14$ and $L_{max} = 8.97$ for smaller QDs and $n = 2.08$, $L_{max} = 29.70$ for larger QDs indicates a degree of sequential binding with some positive cooperativity, which is stronger for the smaller QDs than for larger QDs. For DHLA-QDs, the Hill coefficient between 1.14 and 1.45 and L_{max} between 7.70 and 14.65 is more indicative of negative cooperativity, although it is more difficult to distinguish between sequential and independent binding. At this point, it is important to make a cautionary note on the difference between the values of *K* in **Table 3.1** and the often-reported dissociation constants, K_d, for ligand binding. For $n > 1$, in the case of marked strong cooperativity, $K_d = K^n$. However, since this is not the case here, one must be extremely careful in extracting K_d values for binding of coordinating species to QD surfaces and, likely, for nanoparticles in general.

The mechanistic differences in binding were particularly evident from plotting the probability of dyes to bind as a function of the number of dyes added (**Figure 3.5 c**). It is clearly seen that the probabilities are strongly dependent on the monodentate or bidentate nature of the initial QD ligands, while they are not so dependent on the QD size. The probabilistic aspects of the Hill equation in physicochemical equilibrium applications has been previously examined[29] and are further explored in the context of QD ligand exchange in the Supporting Information. Taken together, these data allow to us postulate a microscopic view of the binding and exchange mechanisms present for each type of ligand coordination. The fact that thiolated dyes bind to DHLA-QDs more readily at low dye:QD ratios than MPA-QDs may be related to the nonlinear geometry of DHLA versus linear MPA resulting in a lower packing density of DHLA on the QD. This may allow the first thiolated dye molecules to bind without having to remove the original ligands. As the surface area increases, dye ligands can bind even easier at lower dye:QD ratios from having more potential binding sites available. For the more densely covered MPA-QDs, the ligands must undergo an exchange process even at low ratios of dye:QD. As more dye ligands are added to the QDs, both types of thiol ligand must now be exchanged, which is easier for the monodentate MPA-QDs than the bidentate DHLA-QDs. However, once the first dyes have bound to the MPA-QD, the positive cooperativity highlights that subsequent dye ligands can bind more easily. This suggests that the binding of the first dyes opens up additional binding sites by facilitating the dissociation of additional MPA ligands, possibly by rotational collisions of the large, bound dye with other MPA ligands, followed by surface ligand rearrangement which opens up additional binding sites and thereby increases the probability of additional dyes to bind. These mechanistic differences are highlighted in **Figure 3.6**.

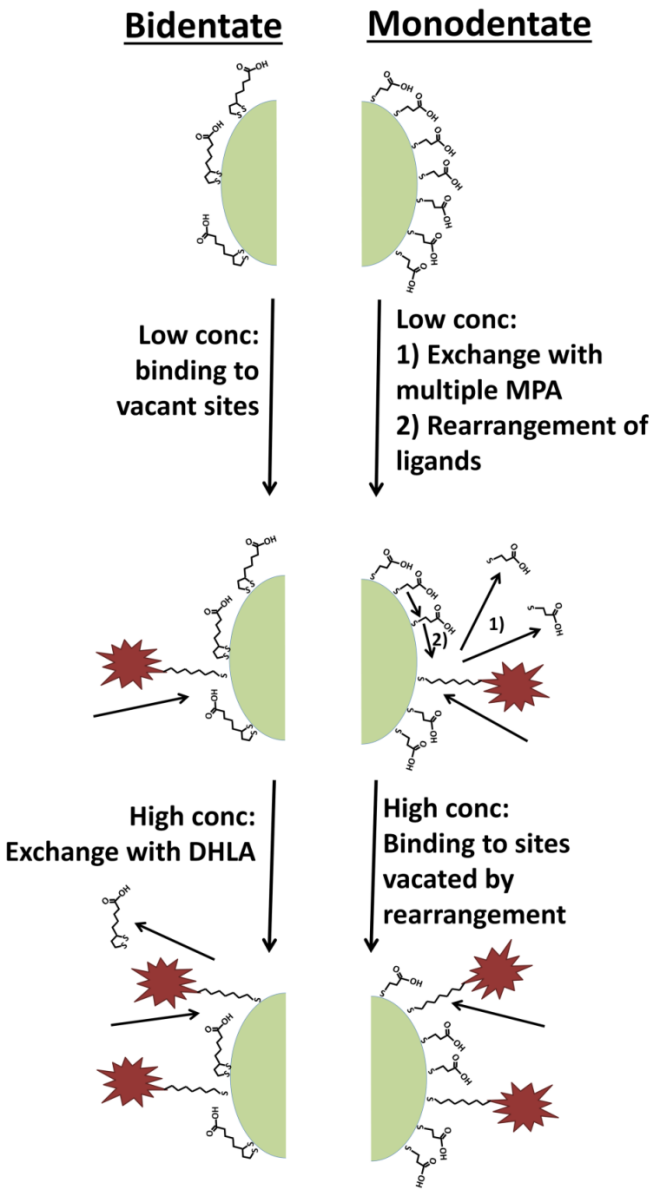

Figure 3.6: Schematic representation of the proposed mechanistic differences in thiolated dye molecules binding and exchanging to DHLA-QDs and MPA-QDs.

As the QDs reach the maximum number of dyes that can bind, L_{max}, the bidentate nature of DHLA limits the total ligands exchanged, although this difference is small for thin-shell QDs that have a total average diameter of 4.3 nm (surface area 58.1 nm^2). For thick-shell QDs, with a total average diameter of 6.8 nm (surface area 145 nm^2) the difference in L_{max} is significant; twice as many thiolated dye ligands can bind to MPA-QDs than DHLA-QDs. For smaller QDs,

the similar saturation level suggests that the limitation is not the number of binding sites available but steric effects from the adsorbed species. The structure of Atto 700 is not published, but the molecular weight of the amine-dye ion, 608 g mol^{-1}, together with the general structure of long wavelength oxazine dyes,[30] and taking into account the linker moiety allows us to postulate a conservatively high estimate of the footprint of the dye to be ~6 nm^2 (i.e., ~ 2 nm × 3 nm). The L_{max} value for the thin-shell QDs of 7-8 dyes per QD is therefore in general agreement with a sterically-limited exchange. Similarly, for the thick-shell QDs, the L_{max} for MPA-QDs is 26, which is also in general agreement with steric limitations. The lower L_{max} for thick-shell DHLA-QDs compared to MPA-QDs indeed highlights that the bidentate nature of the ligand provides reasonable protection to extensive ligand exchange, but only after the already-available surface sites have been taken up. Monodentate ligands will more thoroughly exchange with the thiols in solution until the surface becomes sterically saturated. It is interesting to note that the fact that 2 thiol bonds must be broken to allow a single monodentate ligand to bind reduces the L_{max} by a factor of 2, compared to a simple monodentate-for-monodentate ligand exchange. It will be interesting to see how this scales with larger nanoparticle sizes and thicker shells. One possibility that must be considered is that different shell thicknesses may result in different amounts of Cd-to-Zn on the QD surface, due to imperfect shelling. The surface atom ratio may indeed result in different affinities to ligand functional groups, as previously shown for core-only CdTe.[22] Quantifying this ratio for core-shell QDs is more difficult due to the lack of techniques that probe surface atoms without interference from internal atoms, but will lead to a more thorough understanding of nonspecific binding mechanisms, and will be the focus of future studies.

A major driving force behind this study was to understand the role of the ligand coordination geometry in preventing nonspecific adsorption of thiolated biomolecules in order to

optimize site-specific labeling strategies of proteins using QDs. The use of a thiolated dye as a spectroscopic probe allowed us to focus specifically on quantifying the role of coordination geometry in thiol binding and exchange mechanisms. Biomolecules are far more complicated, and the size, shape, and pI of the biomolecule and pH of the solution are all expected to play a role. Nevertheless, we tested if our model on the role of monodentate versus bidentate ligands can be directly applied to proteins containing free thiols in the form of reduced cysteine groups. We partially reduced a dye-labeled immunoglobulin G (IgG) antibody containing 3 dyes/antibody (AlexaFluor 700 Goat Anti-mouse IgG, A21036, Life Technologies, Carlbad, CA) by mixing 13.2 nmol of TCEP with 0.66 nmol of IgG in 50 μL buffer (100 mM Na_3PO_4, 0.15 M NaCl, 10 mM EDTA, pH 7.2) and reacting for 2 h at 37 °C. We separated reduced IgG from unreduced IgG using a 100kDa Nanosep centrigugal filter (Pall, Port Washington, NY) for 5 min at 5000 rpm. The blue-colored solution from the reduced dye-labeled antibody passed through the membrane, while the unreduced antibody (also blue) remained above the filter. This unreduced antibody was rediluted in additional TCEP/buffer solution (50 μL), and left to react for 2 more hours at 37 °C. Then, the solution was passed through another round of filtration and the second filtrate was combined with the first. Binding to QDs was evaluated by adding 0.1 nmol of the reduced antibody to 0.1 nmol of MPA-QD or DHLA-QD in 100 μL of buffer and left for 2 h at room temperature in the dark. Unbound antibody was separated from QD-antibody conjugates using the 100 kDa centrifugal filter, first by increasing the volume to 220 μL with buffer then centrifuging for 90 s at 5000 rpm. Approximately 170 μL of the solution containing free antibody passed through the filter, leaving 50 μL of the QD-antibody conjugate solution above the filter. This was diluted to 200 μL and another round of centrifugation was completed, to ensure as much of the unbound antibody as possible was removed. For each sample, the

solution was diluted back to 200 µL and the absorption spectra were measured, as shown in **Figure 3.7**. We found that performing more than 2 rounds of separation resulted in aggregation of the QDs, particularly the MPA-QDs. However, under these conditions, any free antibody will have been reduced by a factor of ~17 compared to the QD-antibody conjugates, and thus will not interfere with the assay. It is clear from the absorption spectra that the same concentration of MPA-QDs and DHLA-QDs remained in solution but a smaller dye peak (from the dye-labeled antibody) was observed for the MPA-QDs than for the DHLA-QDs. Specifically, DHLA-QDs contained 35% more antibody per QD than MPA-QDs, highlighting that, at low QD:target ratios, our model for thiol binding to monodentate and bidentate-QDs holds for thiolated biomolecules, although other factors such as size and electrostatics are likely to play a role as well.

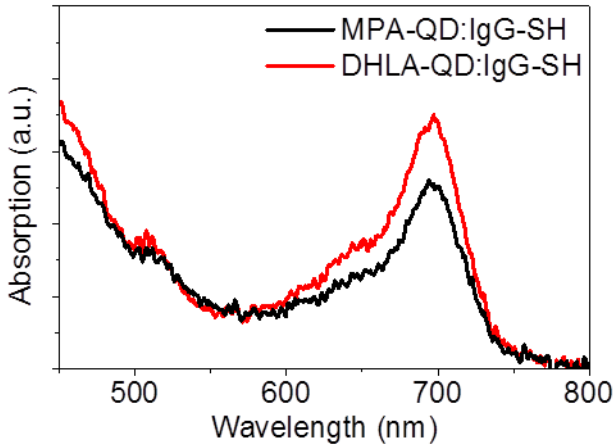

Figure 3.7: Absorption spectra of partially reduced IgG, labeled with AlexaFluor 700, nonspecifically bound to MPA-QDs (black) and DHLA-QDs (red) that were initially mixed at a 1:1 IgG:QD ratio and separated by ultrafiltration.

In summary, we thiolated a near-infrared absorbing dye reporter to use as a spectroscopic probe to examine nonspecific binding of thiol groups to monodentate (MPA)- and bidentate (DHLA)-coated QDs. Surprisingly, we found that, at low dye:QD ratios, DHLA-QDs are worse than MPA-QDs at inhibiting adsorption of thiol ligands but are better as the dye:QD ratio

increases. For small QDs, both types of QDs are able to accommodate approximately the same maximum number of thiolated dye ligands per QD, suggesting steric limitations. As the surface area of the QD increases, bidentate ligands limit the total number of ligands that can be exchanged, thus preventing excessive nonspecific adsorption. Parameters extracted from fitting the data to the Hill equation were used to postulate mechanistic differences in the exchange and binding of thiols to QDs with these two common but different types of surface passivations. We tested this model on a reduced IgG antibody and found that, at 1:1 QD:IgG ratios, monodentate ligands did indeed reduce nonspecific binding to QDs compared to bidentate ligands.

Therefore, to answer the question posed in the title of this manuscript, if it is required to inhibit binding of single molecules at low concentration, such as for labeling proteins for single molecule assays or the ultrasensitive detection of biomarkers, monodentate ligands such as MPA are likely better ligands to render the QDs biocompatible, whereas if limiting the total nonspecific adsorption of biomolecules at high concentrations is the major requirement, such as for labeling overexpressed proteins in cells, bidentate or multidentate ligands such as DHLA are probably better suited. This conclusion may be applicable to other fields of interest in the nano community. For example, if QDs, or nanoparticles in general, are to be used in catalytic applications, the lower ligand density of bidentate ligands such as DHLA may allow for more catalytically-active sites to be exposed to the substrate at low concentrations, but for higher conversion rates at higher substrate concentration, the more labile monodatate ligands such as MPA may allow the QD to become more catalytically active, although it may also reduce colloidal stability. Finally, controlling the ligand coordination geometry on nanoparticles together with the concentration of self-assembling ligand connectors added to solution may allow

for more control over the final geometry of assembled nanostructures by controlling the number of active sites for such ligand connecters to coordinate.

Supporting Information

Mass Spectra of dye before and after modification according to Figure 3.1

MALDI-TOF mass spectra of the as-purchased Atto700-amine and the resulting thiolated dye were acquired on a Bruker UltraflexII Mass Spectrometer (**Figure S3.8 a and b**, respectively). Successful thiolation of the dye was verified by the higher mass peaks corresponding to the dye + SATA (**Figure S3.8 b**, which came off the C-18 HPLC column at a longer retention time as shown in **Figure 3.2** of the main text.

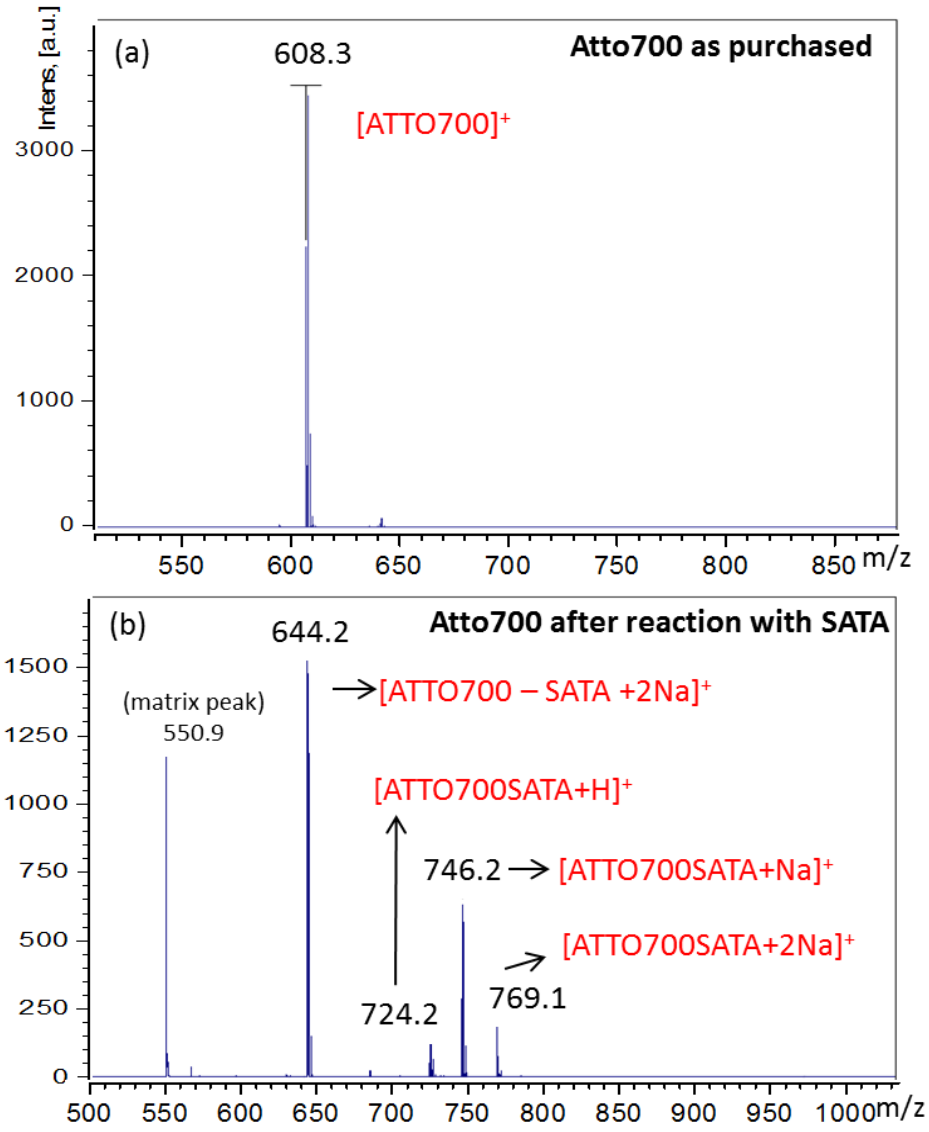

Figure S3.8

Absorption and PL spectra of the original QDs, MPA-QDs and DHLA-QDs with thin and thick shells

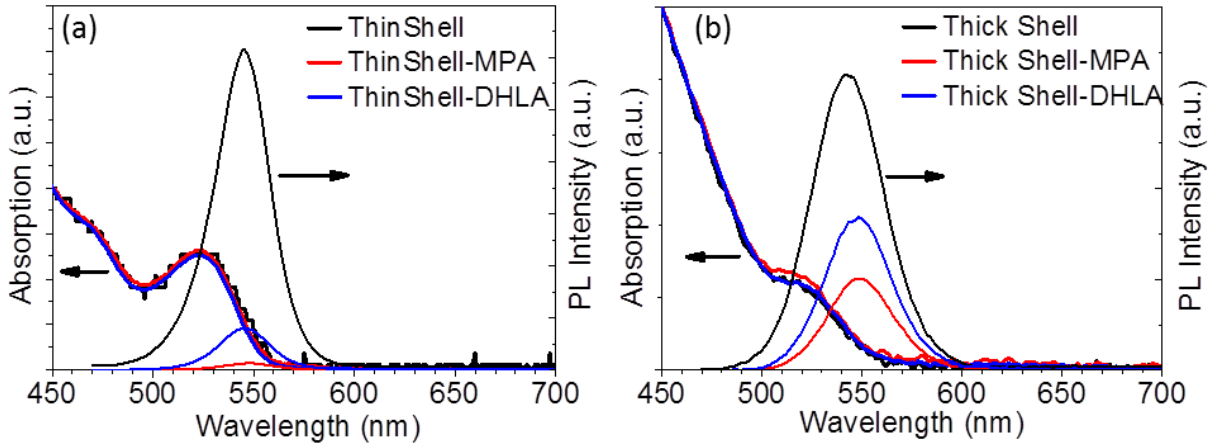

Figure S3.9

Trap emission from some batches of thin-shell QDs

We purchased several batches of core-shell CdSe-ZnS QDs from two different companies; NNLabs, Fayetteville, AR and Ocean Nanotech, Springdale, AR. We purchased their 'standard' 520 nm emitting samples, which were found by TEM to have ~3ML of ZnS shell. We also requested thick-shell QDs as a special order. The ability for thin-shell QDs to undergo ligand exchange without detrimental effects on their emission varied from batch-to-batch, with some samples showing spectra similar to **Figure S3.10**. Samples that showed this trap emission problem were not used for further study.

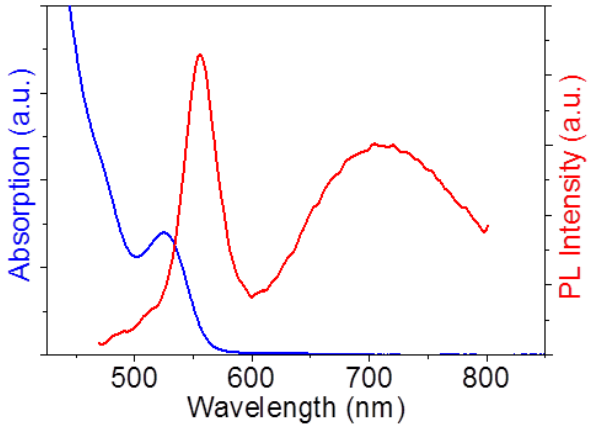

Figure S3.10

Size exclusion chromatography of QD-dye conjugates

Efficient separation of QD and QD-dye conjugates from free dye was accomplished by size exclusion chromatography, as depicted in **Figure S3.11 a**. Example chromatograms for DHLA-QD:added dye ratios of 1:2 and 1:100 are shown in **Figure S3.11 b and c**, respectively. Even when large amounts of free dye are present, efficient separation is possible, ensuring that the resulting absorption and emission spectra are representative of QD-dye conjugates only.

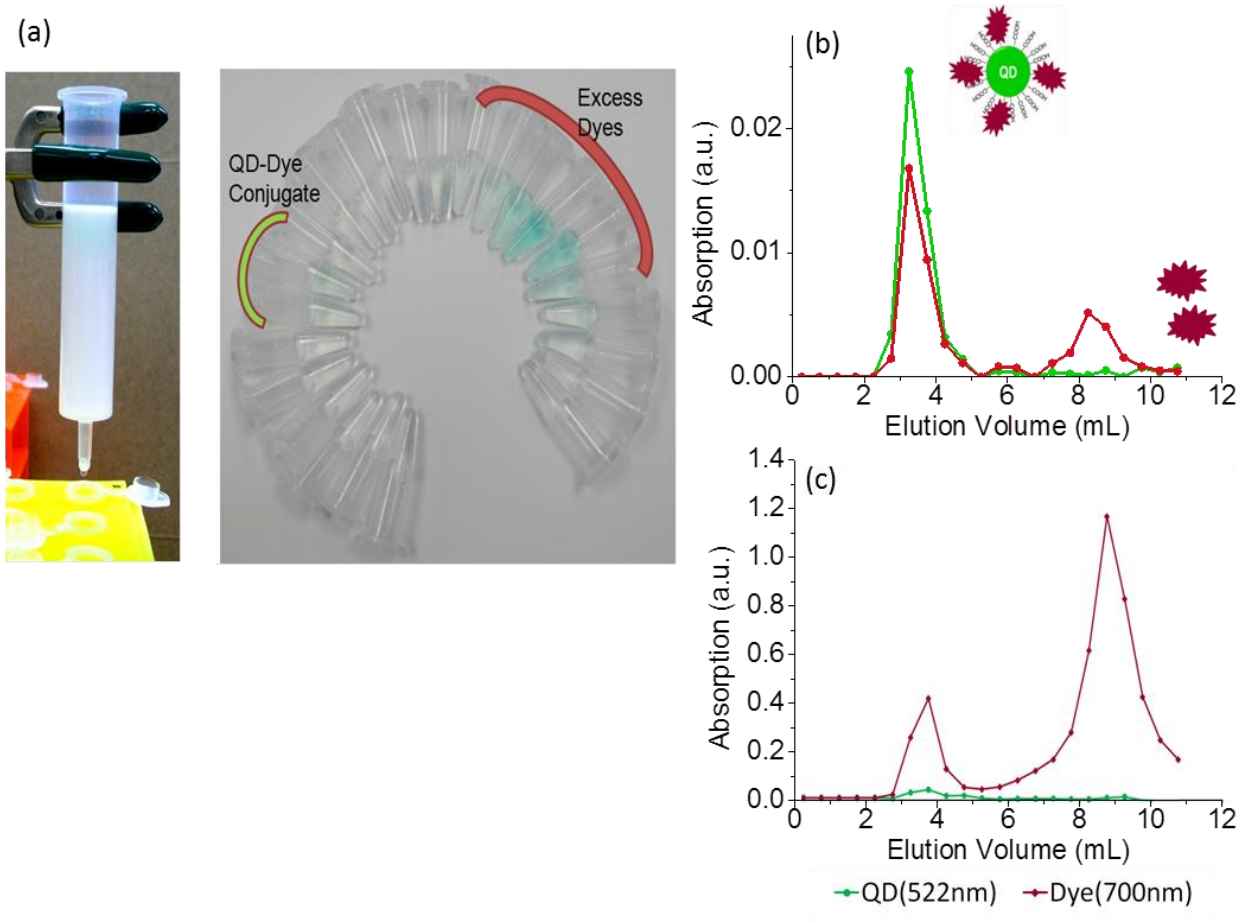

Figure S3.11

Probabilistic Aspects of the Hill equation as applied to thiols binding to QDs

The excellent fits of the thiolated dye binding data to the Hill equation was used to analytically determine the cumulative probability and probability density function for dye binding, as previously shown.[29] Using the notation in the main text, the Hill equation is described by equation **S3.1**

$$y = \frac{L_{max}x^n}{K^n + x^n} \qquad \textbf{(S3.1)}$$

Where L_{max} is the maximum number of ligands that bind to the QD, K is the relative binding strength and n is the Hill coefficient. y is the number of dyes that actually bound for a given number of dyes added, x. The cumulative probability, $P\{X\}$, of dyes binding to their maximum value is therefore given by dividing by L_{max} and rearranging to give equation **S3.2**

$$P\{X\} = 1 - \frac{1}{1+\left(\frac{x}{K}\right)^n} \qquad 0 \le X \le L_{max} \qquad \textbf{(S3.2)}$$

Where X is the average number of dyes bound, up to the maximum value, L_{max}. This is plotted for each QD sample in **Figure S3.12 a**, and is basically just a normalized representation of **Figure 3.5 b** in the main text. The probability density function, *PDF{X}*, is the derivative of equation (**S3.2**),

$$PDF\{X\} = \frac{dP\{X\}}{dx} = \frac{n\left(\frac{x}{K}\right)^n}{x\left(\left(\frac{x}{K}\right)^n + 1\right)^2} \qquad 0 \le X \le L_{max} \qquad \textbf{(S3.3)}$$

Which is plotted in **Figure S3.12 b** as solid lines for each QD sample. The data calculated based on the probability of binding in **Figure 3.5 c** in the manuscript are shown as dashed lines for comparison. To ensure the same scaling, each curve of **Figure 3.5 c** is divided by L_{max} for plotting in **Figure S3.12 b**. As can be seen, the analytically-derived PDFs and the calculated probability of binding are very similar, as would be expected. The probability of binding (**Figure 3.5 c** and the dashed lines of **Figure S3.12 b**) is calculated using the Hill equation fit parameters

to compute the number of dyes attached as a function of the number of dyes added (varying from 0 to 500) and determining the fraction of dyes that bound. The expression based on this calculation is equation (**S3.1**) divided by the number of dyes added, x:

$$Fraction\ that\ Bound = \frac{L_{max}x^n}{x(K^n+x^n)} = \frac{L_{max}\left(\frac{x}{K}\right)^n}{x\left(\left(\frac{x}{K}\right)^n+1\right)} \qquad \textbf{(S3.4)}$$

Comparing equations (**S3.4**) and (**S3.3**) shows the relationship between fraction bound and the probability density function, and are shown as solid and dashed lines of **Figure S3.12 b** (after dividing by the L_{max} scaling parameter). One can see the similarity of the curve shapes, although the PDFs generally overestimate the probability of binding at low concentrations and underestimate it at high concentrations.

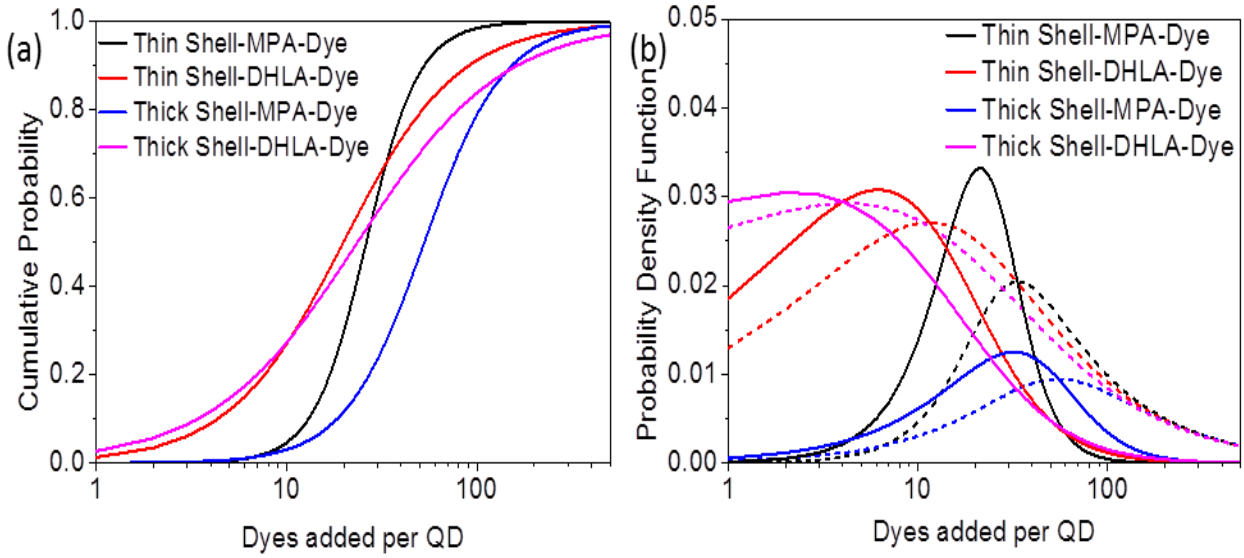

Figure S3.12

3.1 References

1. Chan, W. C.; Nie, S. Quantum Dot Bioconjugates for Ultrasensitive Nonisotopic Detection. *Science* **1998,** 281, (5385), 2016-2018.

2. Bruchez, M.; Moronne, M.; Gin, P.; Weiss, S.; Alivisatos, A. P. Semiconductor Nanocrystals as Fluorescent Biological Labels. *Science* **1998,** 281, 2013-2016.

3. Alivisatos, A. P. The Use of Nanocrystals in Biological Detection. *Nat. Biotechnol.* **2004,** 22, 47-52.

4. Aldana, J.; Wang, Y. A.; Peng, X. Photochemical instability of CdSe nanocrystals coated by hydrophilic thiols. *J. Am. Chem. Soc.* **2001,** 123, (36), 8844-50.

5. Breus, V. V.; Heyes, C. D.; Tron, K.; Nienhaus, G. U. Zwitterionic Biocompatible Quantum Dots for Wide pH Stability and Weak Nonspecific Binding to Cells. *ACS Nano* **2009,** 3, (9), 2573-2580.

6. Breus, V. V.; Heyes, C. D.; Nienhaus, G. U. Quenching of CdSe-ZnS Core-Shell Quantum Dot Luminescence by Water-Soluble Thiolated Ligands. *J. Phys. Chem. C* **2007,** 111, (50), 18589-18594.

7. Wu, X.; Liu, H.; Liu, J.; Haley, K. N.; Treadway, J. A.; Larson, J. P.; Ge, N.; Peale, F.; Bruchez, M. P. Immunofluorescent Labeling of Cancer Marker Her2 and Other Cellular Targets With Semiconductor Quantum Dots. *Nat. Biotechnol.* **2003,** 21, (1), 41-46.

8. Anderson, R. E.; Chan, W. C. W. Systematic Investigation of Preparing Biocompatible, Single, and Small ZnS-Capped CdSe Quantum Dots with Amphiphilic Polymers. *ACS Nano* **2008,** 2, (7), 1341-1352.

9. Gao, X.; Cui, Y.; Levenson, R. M.; Chung, L. W. K.; Nie, S. In vivo cancer targeting and imaging with semiconductor quantum dots. *Nat Biotech* **2004,** 22, (8), 969-976.

10. Dubertret, B.; Skourides, P.; Norris, D. J.; Noireaux, V.; Brivanlou, A. H.; Libchaber, A. In vivo imaging of quantum dots encapsulated in phospholipid micelles. *Science* **2002,** 298, (5599), 1759-62.

11. Kim, S.-W.; Kim, S.; Tracy, J. B.; Jasanoff, A.; Bawendi, M. G. Phosphine Oxide Polymer for Water-Soluble Nanoparticles. *J. Am. Chem. Soc.* **2005,** 127, (13), 4556-4557.

12. Gerion, D.; Pinaud, F.; Williams, S. C.; Parak, W. J.; Zanchet, D.; Weiss, S.; Alivisatos, A. P. Synthesis and Properties of Biocompatible Water-Soluble Silica-Coated CdSe/ZnS Semiconductor Quantum Dots. *J. Phys. Chem. B* **2001,** 105, (37), 8861-8871.

13. Michalet, X.; Pinaud, F. F.; Bentolila, L. A.; Tsay, J. M.; Doose, S.; Li, J. J.; Sundaresan, G.; Wu, A. M.; Gambhir, S. S.; Weiss, S. Quantum Dots for Live Cells, in Vivo Imaging, and Diagnostics. *Science* **2005,** 307, 538-544.

14. Yu, W. W.; Chang, E.; Drezek, R.; Colvin, V. L. Water-soluble quantum dots for biomedical applications. *Biochem. Biophys. Res. Commun.* **2006,** 348, (3), 781-786.

15. Nida, D. L.; Nitin, N.; Yu, W. W.; Colvin, V. L.; Richards-Kortum, R. Photostability of quantum dots with amphiphilic polymer-based passivation strategies. *Nanotechnology* **2008,** 19, (3), 035701.

16. Zhang, Y.; Clapp, A. Overview of Stabilizing Ligands for Biocompatible Quantum Dot Nanocrystals. *Sensors* **2011,** 11, (12), 11036-11055.

17. Mattoussi, H.; Mauro, J. M.; Goldman, E. R.; Anderson, G. P.; Sundar, V. C.; Mikulec, F. V.; Bawendi, M. G. Self-Assembly of CdSe-ZnS Quantum Dot Bioconjugates Using an Engineered Recombinant Protein. *J. Am. Chem. Soc.* **2000,** 122, (49), 12142-12150.

18. Pinaud, F.; King, D.; Moore, H.-P.; Weiss, S. Bioactivation and Cell Targeting of Semiconductor CdSe/ZnS Nanocrystals with Phytochelatin-Related Peptides. *J. Am. Chem. Soc.* **2004,** 126, 6115-6123.

19. Uyeda, H. T.; Medintz, I. L.; Jaiswal, J. K.; Simon, S. M.; Mattoussi, H. Synthesis of Compact Multidentate Ligands to Prepare Stable Hydrophilic Quantum Dot Fluorophores. *J. Am. Chem. Soc.* **2005,** 127, (11), 3870-3878.

20. Hermanson, G. T., *Bioconjugate Techniques*. Second ed.; Academic Press: San Diego, CA, 2008.

21. Kuzmenkina, E. V.; Heyes, C. D.; Nienhaus, G. U. Single molecule Förster resonance energy transfer study of protein dynamics under denaturing conditions. *Proc. Natl. Acad. Sci. U. S. A.* **2005,** 102, 15471-15476.

22. Omogo, B.; Aldana, J. F.; Heyes, C. D. Radiative and Nonradiative Lifetime Engineering of Quantum Dots in Multiple Solvents by Surface Atom Stoichiometry and Ligands. *J. Phys. Chem. C.* **2013,** 117, 2317–2327.

23. Yu, W. W.; Qu, L.; Guo, W.; Peng, X. Experimental Determination of the Extinction Coefficient of CdTe, CdSe, and CdS Nanocrystals. *Chem. Mater.* **2003,** 15, (14), 2854-2860.

24. Clapp, A. R.; Goldman, E. R.; Mattoussi, H. Capping of CdSe-ZnS quantum dots with DHLA and subsequent conjugation with proteins. *Nat Protoc* **2006,** 1, (3), 1258-66.

25. Leatherdale, C. A.; Woo, W. K.; Mikulec, F. V.; Bawendi, M. G. On the Absorption Cross Section of CdSe Nanocrystal Quantum Dots. *J. Phys. Chem. B* **2002,** 106, (31), 7619-7622.

26. Jasieniak, J.; Smith, L.; Embden, J. v.; Mulvaney, P.; Califano, M. Re-examination of the Size-Dependent Absorption Properties of CdSe Quantum Dots. *J. Phys. Chem. C* **2009,** 113, (45), 19468-19474.

27. Dong, C.; Ren, J. Measurements for molar extinction coefficients of aqueous quantum dots. *Analyst* **2010,** 135, (6), 1395-1399.

28. Weiss, J. N. The Hill equation revisited: uses and misuses. *FASEB J.* **1997,** 11, (11), 835-41.

29. Goutelle, S.; Maurin, M.; Rougier, F.; Barbaut, X.; Bourguignon, L.; Ducher, M.; Maire, P. The Hill equation: a review of its capabilities in pharmacological modeling. *Fundam. Clin. Pharmacol.* **2008,** 22, (6), 633-648.

30. Gomez-Hens, A.; Aguilar-Caballos, M. P. Long-wavelength fluorophores: new trends in their analytical use. *TrAC-Trend. Anal. Chem.* **2004,** 23, (2), 127-136.

3.2 Appendix I

UNIVERSITY OF ARKANSAS

J. William Fulbright College of Arts and Sciences
Chemistry and Biochemistry

To whomever it may concern

This is to certify that Ms. Hiroko Takeuchi is the first author of the paper mentioned below and has contributed about 75% of the work reported in this paper

Hiroko Takeuchi, Benard Omogo, and Colin D. Heyes. Are Bidentate Ligands Really Better than Monodentate Ligands For Nanoparticles? Nano Letters, (2013) **13**, 4746-4752

Colin D. Heyes

Major Advisor

CHEM 119 • 1 University of Arkansas • Fayetteville, AR 72701-1201 • 479-575-4601 • Fax: 479-575-4049 • http://chemistry.uark.edu/

3.3 Appendix II

11/26/13 RightsLink® by Copyright Clearance Center

Copyright Clearance Center RightsLink®

Home | Account Info | Help

ACS Publications High quality. High impact.

Title: Are Bidentate Ligands Really Better than Monodentate Ligands For Nanoparticles?

Author: Hiroko Takeuchi, Benard Omogo, and Colin D. Heyes

Publication: Nano Letters

Publisher: American Chemical Society

Date: Oct 1, 2013

Copyright © 2013, American Chemical Society

Logged in as: Colin Heyes

LOGOUT

PERMISSION/LICENSE IS GRANTED FOR YOUR ORDER AT NO CHARGE

This type of permission/license, instead of the standard Terms & Conditions, is sent to you because no fee is being charged for your order. Please note the following:

- Permission is granted for your request in both print and electronic formats, and translations.
- If figures and/or tables were requested, they may be adapted or used in part.
- Please print this page for your records and send a copy of it to your publisher/graduate school.
- Appropriate credit for the requested material should be given as follows: "Reprinted (adapted) with permission from (COMPLETE REFERENCE CITATION). Copyright (YEAR) American Chemical Society." Insert appropriate information in place of the capitalized words.
- One-time permission is granted only for the use specified in your request. No additional uses are granted (such as derivative works or other editions). For any other uses, please submit a new request.

BACK | CLOSE WINDOW

Copyright © 2013 Copyright Clearance Center, Inc. All Rights Reserved. Privacy statement.
Comments? We would like to hear from you. E-mail us at customercare@copyright.com

https://s100.copyright.com/AppDispatchServlet 1/1

Chapter 4: Ensemble and Single Molecule Spectroscopic Analysis of QD-Dye Conjugates

4.1 Introduction

In the previous chapter, the binding and exchange of single thiolated dyes with monodentate and bidentate coordination was discussed based on the results of absorption spectroscopy and Hill equation analysis, which revealed that the ligand coordination geometry affected the type of binding scheme for thiolated target molecules; QD-MPA was more consistent with sequential positive cooperative binding, while QD-DHLA showed indications of independent negative cooperative binding, although this was less conclusive. In addition to the discovery of binding mechanism differences, the final conjugates (QD-Dye) were further studied by photoluminescence spectra for FRET analysis and lifetime measurements at both ensemble and single molecule levels to gain more knowledge about the non-specific binding of thiolated target molecules to individual QDs.

4.2 Experimental Methods

4.2.1 *Photoluminescence (PL)*

PL spectra of fractions containing the QD-Atto 700 conjugates were obtained using the fluorometer. Due to the low concentration of the conjugates following size exclusion column purification, the PL spectra were normalized without adjusting the absorption at excitation wavelength (450 nm); instead, they were normalized by dividing each spectrum by the absorption value at 450 nm. The maximum intensity at QDs emission of control reaction containing just QDs (I_{QD}) and the conjugates fractions ($I_{QD\text{-}Dye}$) were employed to calculate the FRET efficiency (E) using the following equation.

$$E = 1 - \frac{I_{QD-dye}}{I_{QD}} \quad \textbf{(4.1)}$$

The FRET efficiency for each sample was plotted against the dyes attached per QDs that were calculated from the absorption spectra in the previous chapter. This graph enabled us to see the trends in the effect on the FRET efficiency upon binding and exchange of thiolated dye ligands at ensemble level.

4.2.2 *Fluorescence Lifetime*

In addition to the analysis at the ensemble level, the QD-Dye conjugates were further studied at a single molecule level by measuring the lifetime of the conjugates. In this part, the fractions obtained from the sample in which the QD:Dye ratio that was added was 1:1 due to the results indicating that on average, there was 0.18 dye ligands exchanged on one QD.

The data acquisition of single molecule lifetime traces was conducted by another graduate student, Derrel Walters, using the Picoquant MicroTime 200 microscope equipped with 485 nm pulsed excitation (PDL-485). For this single molecule study, the samples were diluted to pico-molar concentration and were mixed with 4% poly (vinyl alcohol) (PVA, Alfa Aesar). The mixture was applied to a glass coverslip (Propper Manufacturing) and spin-coated. Images were captured by scanning the piezo stage pixel-by-pixel, which was used to ensure that single QDs were separated by more than the point spread function (PSF) of the collected emitted light. The time-correlated single photon counting (TCSPC) data was obtained by randomly scanning points that were spaced greater than this PSF. This method allowed us to obtain the lifetimes of both QDs with high and low FRET efficiencies without biasing toward the brighter QDs. The parameters of TCSPC data acquisition were 4096 channels with 64 ps time resolution per channel at 3.6 MHz laser repetition rate with a 60-second integration time. Each trace was checked to identify the points that showed only the instrument response function to remove the

background fluorescence. Altogether 104 single QD lifetimes were measured and summarized in a histogram.

In addition to the single molecule lifetime measurement, the ensemble lifetimes were also measured to gain more insight to the FRET efficiencies of each sample. The concentration of the samples was reduced to pico-molar concentratios, but this time the measurement was performed with the QDs diffusing in solution. Three examples of lifetime traces are presented in this chapter.

For both ensemble and single QDs, the fluorescence lifetimes were measured using a pulsed laser operating at 485 nm, 15 μW and 5 MHz for excitation and focused though the objective (PlanApo 63xW, Olympus) to a diffraction limited spot. Before the emission was collected by a Single Photon Counting Avalanche Diode (PDM series, Microphotonic devices, Bolzano, Italy), the QDs emissions passed through a ET560/40x filter. The data was exported as analyzed in the SymPhoTime (version 5.3.2, Picoquant GmbH) software and exported as text files to produce the figures using OriginPro 8 software.

4.3 Results and Discussion

4.3.1 *Photoluminescence (PL)*

The emission spectra of all the product solutions were measured to analyze their FRET efficiencies. The overlay of photoluminescence spectra upon excitation at 450nm of each QD-Atto 700 conjugate is shown in **Figure 4.1 a**. The intensity of QDs' emission, the peak at around 540nm, decreased as more dyes were added to the conjugation mixture, indicating the presence of FRET between QDs (donor) and Atto 700 (acceptor) , which was also observable under a hand-held UV light (365 nm), shown in **Figure 4.1 a, inset**. The first emission peak from QDs

should decrease as more FRET occurs, and the second emission peak from acceptor, Atto 700, should increase. However, the PL from the acceptor did not increase as more dyes were attached to the surface of QDs. According to the manufacture product information, Atto 700 fluorescence is efficiently quenched by electron donors, which may include carboxylate groups of the water solubilizing ligands on QDs.[1, 2] FRET efficiencies were calculated using (**4.1**) by using the QDs' emission peaks and plotted against the number of dyes attached (**Figure 3.5 b**) as determined by the absorption values (**Figure 4.1 b**). For all the samples, FRET increased drastically and reached the saturation efficiency when just few dyes were attached per QDs; for thin shelled-QD, 2 dyes, and for thick shelled-QD, 5 dyes were enough to cause their maximum FRET efficiency. There was also a trend between the types of ligand used. QDs exchanged with DHLA ligands reached to 100% FRET efficiency with slightly less dyes attached compared to exchange with MPA ligands. The saturation of FRET efficiency at a single or a few ligands attached has been previously reported; for 4 nm CdSe/ZnS QDs, 3.4-dye attachment was enough to reach its maximum FRET efficiency.[3]

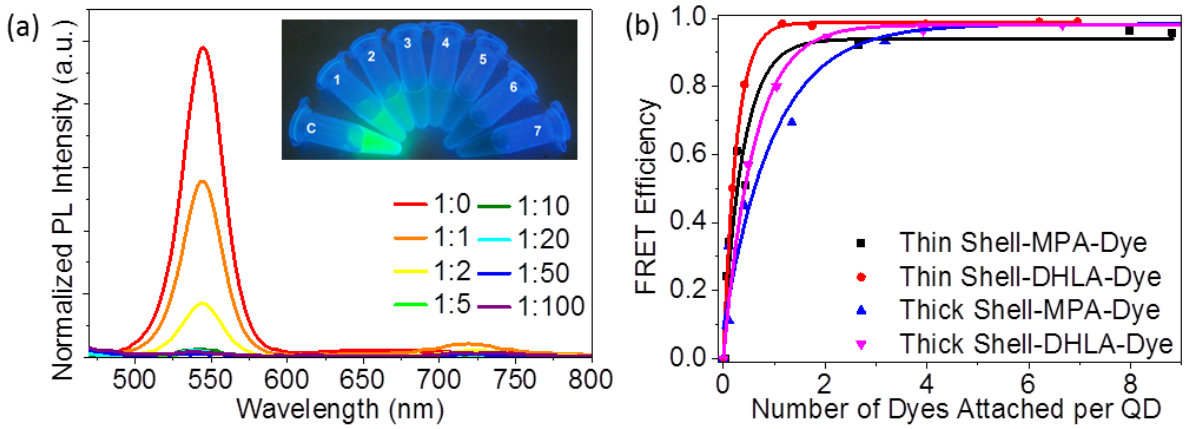

Figure 4.1: (a) En example of Photoluminescence Spectra overly of Thin-Shell-DHLA set. The inset shows dye quenching in the environment of the QD surface (inset). (b) Ensemble FRET efficiency as a function of number of dyes bound to each QD.

Several researchers have investigated FRET from QDs to organic fluorophores due to its sensitivity to the distance between the donor and acceptor, which can reveal the binding interactions.[4] The FRET efficiency, E, can be expressed in terms of distance (*d*), from the center of the donor to the center of the acceptor, and the number of dyes attached (*n*) according to the equation,

$$E = \frac{n}{n+\left(\frac{d}{R_0}\right)^6} \quad \textbf{(4.2)}$$

where R_0 is the Förster distance, the distance which yields 50 % of the energy transfer. The Förster distance depends on various parameters: the relative orientation of the donor and acceptor dipoles (κ), quantum yield of the donor (φ_D), the spectral overlap integral of donor emission and acceptor absorption (I), and a function of the refractive index of the medium (n_D).

$$R_0{}^6 = \frac{9000(ln10)\kappa^2\varphi_D}{N_A 128\pi^5 n_D{}^4} I \quad \textbf{(4.3)}$$

where κ is commonly assumed to be 2/3 for randomly oriented dipoles in case of QDs consistent with rapid statistical averaging of all orientations within the lifetime of the excited state. It is necessary to make a couple more assumptions for the refractive index of ZnS shell, ligands, and the solvent in order to estimate the value of R_0. In the case of Thin-Shell-DHLA, about 1 nm of thin ZnS layer, 0.5 nm of organic DHLA capping, and 1 nm of water solvent were found to have 2.4, 1.5 and 1.33 refractive indices, respectively[5, 6], which approximated the averaged n_D to be 1.8. Together with 10% for the ensemble quantum yield of QD (φ_D) and the spectra overlap (I) calculated from the integral of donor emission and acceptor absorption in terms of dye extinction coefficient, R_0 value was estimated to be 30 Å for Thin Shell-DHLA.

4.3.2 *Single Molecule Spectroscopy*

In comparison to ensemble FRET analysis, FRET was measured at single molecule level by measuring individual fluorescence lifetimes of QDs (**Figure 4.2**). For this study, the sample

that showed an average binding of 0.18 dyes per Thin Shell-DHLA-QD at the ensemble level was used. This is the sample that was prepared by mixing Thin Shell-DHLA to Atto 700-SH in a 1:1 ratio, thus showing an 18% average probability of a single dye to bind at the ensemble level. From this sample, the fluorescence lifetimes of 104 randomly-selected conjugates were measured individually and summarized in a histogram (**Figure 4.2 a**). The distributions of lifetimes were fitted to Gaussian functions which provide a realistic approximation to the statistical distribution of dyes binding. **Figure 4.2 a** showed three clear distributions of lifetime; 14.1 % of all the QDs measured had 13.5 ns of lifetime on average, 51.1 % with 8.9 ns, and 34.8 % with 4.7 ns. The average lifetime of a control sample containing only QDs without any dyes present was 12.8 ns, which enabled us to assign the species with 13.5 ns of average lifetime to Thin-Shell-DHLA without any dyes bound (**Figure 4.2 b**). The sample with 0.18 dyes per QD at ensemble level showed 7.9 ns of lifetime, which corresponds to the central peak in the histogram, indicating that it is the species with one dye attached to the QD. Likewise, the distribution with short lifetime is assigned to be the spices with two or more dyes attached to a QD.

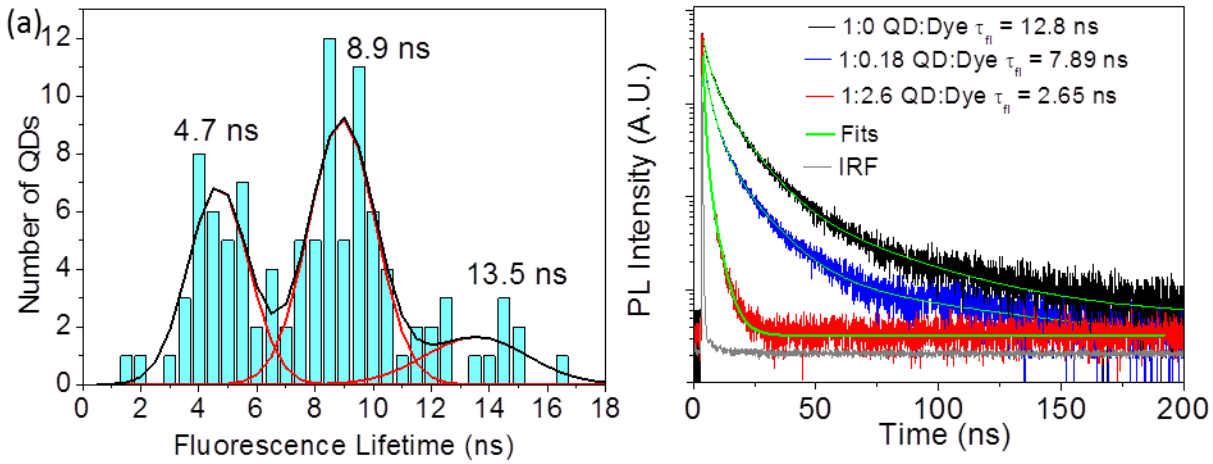

Figure 4.2: (a) Three distributions of single QD lifetimes from one sample produced by mixing 1:1 Thin-Shell-DHLA to dye with Gaussian functions. (b) Average lifetime traces of three different sample containing 0,1, and more than two dyes to a QD (black, blue, and red, respectively).

The probabilities of three species were predicted using Poisson distribution function which assumes a non-cooperative independent binding scheme. The percentages were predicted using the average binding number of 0.18 dyes per QD, measured in chapter 3. The comparison between the measured and Poisson-predicted probabilities of each species is summarized in **Table 4.1**. The differences in the measured versus predicted probabilities suggests that binding is non-Poissonian and highlights the complexity in relating single particle and ensemble data. The fact that we measured higher than expected probabilities for 1 or more dyes to bind could be indicative of positive cooperativity. A previous report observed that binding of His-tagged target molecules to DHLA-QDs did follow Poisson statistics[7], suggesting that the binding group of the target (bio)molecule (and/or its size) plays a major role in determining the cooperativity of binding as well as the ligand coordination geometry.

	Numbers of Dyes Bound		
	0	1	≥2
Experimental	14.1%	51.1%	34.8%
Predicted <N>=0.18	84%	15%	1%

Table 4.1: Comparison between probabilities of three species. Experimental values are compared with the numbers predicted from Poisson distribution with average binding number 0.18 obtained from FRET ensemble experiment.

Even though the three fluorescence distributions were assigned using the ensemble-averaged fluorescence lifetimes decays, there were discrepancies in relating ensemble and single particle FRET efficiencies. One possible explanation for this discrepancy may be due to the blinking of QDs, which is an environment-sensitive phenomenon of fluorescence emission switching between on (fluorescing radiative pathway) and off (non-fluorescing nonradiative pathway) states.[8, 9] The difference in quantum yield (QY) of QDs at ensemble and single particle

levels due to blinking and dark fraction formation of QDs has been reported previously.[9-11] Furthermore, CdSe/ZnS QDs can exhibit gray state emission which is a lower energy emission lying between on and off state emission intensities[9, 12], implying that even at the single molecule level, QDs' emission can vary, which would affect the R_0 values from event-to-event.[10, 13, 14] At the ensemble level, the QDs in each of dark, gray and bright states are included in the measurement; while, at single molecule level, only bright emitting QDs are measured. All these variations contribute to the deviation of the averaged lifetime values from single particle lifetimes. In order to fully discuss this complexity, further work is needed, which is outside of the scope of this research and is the focus for future investigations.

4.4 Conclusion

The single molecule lifetime measurement showed three lifetime distributions, indicating there were three difference species present for the Thin-Shelled-DHLA-QD sample that was exposed to a 1:1 ratio of QD:dye. These species were assigned to QD-DHLA with no dyes attached, QD-DHLA with one dye attached, and QD-DHLA with 2 or more dyes attached, respectively. The data from chapter 3 suggested that QD-DHLA may show negative cooperativity, although it was not conclusive. The lack of agreement with Poisson statistics towards observing higher dye:QD ratios than expected suggests that there may, in fact, be a degree of positive cooperativity in the binding mechanism, although more work is needed to confirm this. Furthermore, comparing the single molecule fluorescence results to the ensemble level revealed inconsistencies that suggests that the FRET may vary from QD-to-QD and from event-to-event within the same sample, possibly a result of blinking and the dark fraction

formation. In order to more accurately describe this discrepancy, further investigations are currently being continued by a fellow researcher.

4.5 References

1. Product Information: ATTO 700. GmbH, A.-T., Ed. Revised: 2013-02-22.

2. Breus, V. V.; Heyes, C. D.; Nienhaus, G. U., Quenching of CdSe-ZnS core-shell quantum dot luminescence by water-soluble thiolated ligands. *Journal of Physical Chemistry C* 2007, 111, 18589-18594.

3. Shivkumar, M. A.; Inamdar (Doddamani), L. S.; Rabinal, M. H. K.; Mulimani, B. G.; Advi Rao, G. M.; Inamdar, S. R., FRET from CdSe/ZnS Core-Shell Quantum Dots to Fluorescein 27 Dye. *Open Journal of Physical Chemistry* 2013, 3, 9.

4. Clapp, A. R.; Medintz, I. L.; Mauro, J. M.; Fisher, B. R.; Bawendi, M. G.; Mattoussi, H., Fluorescence resonance energy transfer between quantum dot donors and dye-labeled protein acceptors. *Journal of the American Chemical Society* 2004, 126, 301-310.

5. Bond, W. L., Measurement of the Refractive Indices of Several Crystals. *Journal of Applied Physics* 1965, 36, 4.

6. Li, H. H., REFRACTIVE-INDEX OF ZNS, ZNSE, AND ZNTE AND ITS WAVELENGTH AND TEMPERATURE DERIVATIVES. *Journal of Physical and Chemical Reference Data* 1984, 13, 103-150.

7. Pons, T.; Medintz, I. L.; Wang, X.; English, D. S.; Mattoussi, H., Solution-Phase Single Quantum Dot Fluorescence Resonance Energy Transfer. *Journal of the American Chemical Society* 2006, 128, 15324-15331.

8. Durisic, N.; Wiseman, P. W.; Grutter, P.; Heyes, C. D., A Common Mechanism Underlies the Dark Fraction Formation and Fluorescence Blinking of Quantum Dots. *Acs Nano* 2009, 3, 1167-1175.

9. Durisic, N.; Godin, A. G.; Walters, D.; Grutter, P.; Wiseman, P. W.; Heyes, C. D., Probing the "Dark" Fraction of Core-Shell Quantum Dots by Ensemble and Single Particle pH-Dependent Spectroscopy. *Acs Nano* 2011, 5, 9062-9073.

10. Ebenstein, Y.; Mokari, T.; Banin, U., Fluorescence quantum yield of CdSe/ZnS nanocrystals investigated by correlated atomic-force and single-particle fluorescence microscopy. *Applied Physics Letters* 2002, 80, 4033-4035.

11. Yao, J.; Larson, D. R.; Vishwasrao, H. D.; Zipfel, W. R.; Webb, W. W., Blinking and nonradiant dark fraction of water-soluble quantum dots in aqueous solution. *Proceedings of the National Academy of Sciences of the United States of America* 2005, 102, 14284-14289.

12. Zhao, J.; Nair, G.; Fisher, B. R.; Bawendi, M. G., Challenge to the Charging Model of Semiconductor-Nanocrystal Fluorescence Intermittency from Off-State Quantum Yields and Multiexciton Blinking. *Physical Review Letters* 2010, 104.

13. Fomenko, V.; Nesbitt, D. J., Solution Control of Radiative and Nonradiative Lifetimes: A Novel Contribution to Quantum Dot Blinking Suppression. *Nano Letters* 2007, 8, 287-293.

14. Montiel, D.; Yang, H., Observation of correlated emission intensity and polarization fluctuations in single CdSe/ZnS quantum dots. *Journal of Physical Chemistry A* 2008, 112, 9352-9355.

Chapter 5: Conclusions

In summary, this research has explored the ligand chemistry on the surface of CdSe/ZnS core/shell quantum dots (QDs). A new ligand coating for QDs was developed to enhance the aqueous colloidal stability. Photocrosslinkable diacetylene (DA) ligands were introduced during the ligand exchange reaction to water-solubilize QDs. The QD-DA showed significantly greater colloidal stability in water compared to the commonly-used, non-crosslinkable control, mercaptopropionic acid (MPA), QD-MPA. Interestingly, although UV light facilitated crosslinking, it also resulted in the aggregation of QD-DA quicker than samples not exposed to UV crosslinking, but exposed to visible light. The lower colloidal stability of QD-DA after UV exposure is suspected to be the result of photooxidation of thiol groups on the surface of QDs resulting in ligand dissociation that competes with crosslinking. Without UV exposure, but under visible light, improved crosslinking is postulated to occur by a QD-catalyzed mechanism. The low-energy visible light is absorbed by the QD, which then initiates crosslinking, presumably by electron transfer between the QD to the DA ligand, without the competing UV-induced ligand dissociation pathway. This finding will be particularly beneficial for long-term biological labeling studies because of the improved colloidal stability, while at the same time maintaining a smaller overall hydrodynamic size compared to the common amphiphilic polymer-coated QDs that are currently commercially available.

In addition to the development of a new photocrosslinkable ligand, the mechanistic differences in how the coordination geometry of the more common monodentate (MPA) and bidentate (DHLA) ligands affected the binding and exchange of thiolated target molecules was uncovered by engineering a near-infrared thiolated dye (Atto 700-SH) to act as a novel spectroscopic probe. It is widely considered that bidentate ligands are better ligands for

nanoparticles, so we tested this assertion and found surprising results. From the absorption spectra, the number of thiolated dyes that bound to each ligand-functionalized QD were calculated and analyzed using the Hill equation parameters. The results indicated that when there was a low concentration of thiolated dye added to the MPA- or DHLA-QDs, DHLA-QDs resulted in more non-specific adsorption of Atto 700, which we attribute to the lower packing denisty of bidentate DHLA on the surface of QDs compared to the monodenate MPA. However, the DHLA-QDs showed more resistance to non-specific adsorption when there were more Atto 700 dyes present in the reaction mixture, where DHLA ligand desorption was necessary for more thiolated dyes to bind. In contrast, the close packing of monodenate MPA ligands on the surface of QDs, which inhibiting from dyes to bind at lower concentrations. When the concentration of thiolated dye ligands was increased, MPA was easier to exchanges with dyes due to the monodentate linkage, which resulted in an increase in the numbers of dyes bound. These mechanistic differences are evidenced in the degrees of cooperativity extracted from the Hill equation, which depended on ligand type but not QD size. These differences were then shown to translate to the reaction of QDs with target thiolated biomolecules, in the form of reduced antibodies IgG-SH. This result promises to be important for the application of QDs in bioimaging applications, since resistance to non-specific adsorption of thiolated biomoelcules will allow for more efficient specific bioconjugation reactions.

Additionally, FRET analysis at the ensemble and single particle level showed the existence of various QD:dye species from the mixture in which a low concentration of thiolated dyes was added to QDs. From the single molecule measurements, three distributions of fluorescence lifetimes were monitored, assigned to QDs without any dyes, QDs with one dye

attached, and QDs with more than two dyes attached. Analysis of this data suggested that the distribution is not Poissonian, and there may be a positive cooperative binding mechanism.

The discoveries in this thesis will be advantageous for researchers who employ water-solubilized QD (CdSe/ZnS) in their research, particularly for controlling number of binding molecules and for performing long term measurements that require a small colloidal size but high colloidal stability. If one requires to minimize the non-specific binding of thiolated target molecules to QDs at low concentrations, the more closely packed monodentate ligand coatings would be preferred. However, if the concentration of thiolated target molecules is high, the degree of non-specific binding is inhibited more using bidentate ligands such as DHLA. Using the above concept, it should become possible to achieve one-to-one bioconjugation with QDs by introducing a specific linker such as BMPH (*N*-β-Maleimidopropionic acid hydrazide·TFA) to specifically target the cysteine groups in biomolecules while at the same time controlling non-specific adsorption, leading to an improvement in the design of specifically-targeted QD fluorescent probes.